DOI: 10.1002/cmdc.200900390

3-Heterocycle-Phenyl *N*-Alkylcarbamates as FAAH Inhibitors: Design, Synthesis and 3D-QSAR Studies

Heikki Käsnänen,[a, c] Mikko J. Myllymäki,[b] Anna Minkkilä,[a] Antti O. Kataja,[b] Susanna M. Saario,[a, d] Tapio Nevalainen,[a] Ari M. P. Koskinen,[b] and Antti Poso*[a]

Carbamates are a well-established class of fatty acid amide hydrolase (FAAH) inhibitors. Here we describe the synthesis of *meta*-substituted phenolic *N*-alkyl/aryl carbamates and their in vitro FAAH inhibitory activities. The most potent compound, 3-(oxazol-2yl)phenyl cyclohexylcarbamate (**2a**), inhibited FAAH with a sub-nanomolar IC_{50} value ($IC_{50} = 0.74$ nM). Additionally, we developed and validated three-dimensional quantitative structure–activity relationships (QSAR) models of FAAH inhibition combining the newly disclosed carbamates with our previously published inhibitors to give a total set of 99 compounds. Prior to 3D-QSAR modeling, the degree of correlation between FAAH inhibition and in silico reactivity was also established. Both 3D-QSAR methods used, CoMSIA and GRID/GOLPE, produced statistically significant models with coefficient of correlation for external prediction (R^2_{PRED}) values of 0.732 and 0.760, respectively. These models could be of high value in further FAAH inhibitor design.

Introduction

The endocannabinoids constitute a class of endogenous lipid transmitters that includes *N*-arachidonoylethanolamine (anandamide, AEA)[1] and 2-arachidonoylglycerol (2-AG).[2,3] They bind to and activate both cannabinoid receptors, CB_1[4,5] and CB_2,[6] inducing several beneficial therapeutic effects[7] such as analgesia,[8] anxiolysis,[9] increase of appetite[10] and reduction of intraocular pressure.[11] In addition, the activation of CB_2 receptors is involved in the decrease of inflammation, lowering of blood pressure, and suppression of peripheral pain.[12] However, the cannabimimetic effects of AEA and 2-AG remain weak and transient in vivo owing to their rapid inactivation by the hydrolytic enzymes fatty acid amide hydrolases (FAAH,[13] EC 3.5.1.4, and FAAH-2[14]) and monoglyceride lipase (MGL, EC 3.1.1.23, also called monoacylglycerol lipase (MAGL)),[15] respectively. Thus, development of effective FAAH and MGL inhibitors, which could enhance the tonic actions of AEA and 2-AG, respectively, has gained a lot of interest within several research groups (for excellent Review articles, see Reference [16]).

The endocannabinoid signaling system is activated upon demand, beginning from endocannabinoid biosynthesis in postsynaptic neurons and ending in their rapid cellular reuptake and enzymatic degradation.[17,18] FAAH has been established as the main metabolizing enzyme responsible for the degradation of AEA. A number of potent inhibitors of this serine hydrolase have been previously reported, such as α-ketoheterocycles,[19] carbamates such as cyclohexylcarbamic acid biphenyl-3-yl ester (URB597),[20] piperine/piperazine ureas,[21] (thio)-hydantoins,[22] and most recently, benzothiazole-based sulfonyls,[23] boronic acids,[24] and oxadiazolones.[25] Of these, some classes have also demonstrated favorable FAAH activity, selectivity and therapeutic effects in vivo.[20,21,26]

The main enzyme responsible for the inactivation of 2-AG in the brain is MGL.[14,27,28] It has been found to be sensitive to nonspecific serine hydrolase inhibitors,[14,28,29] and sulfhydryl-specific compounds.[14,28,30–32] To date, only one compound has been reported to display high efficacy as well as selectivity against MGL. This compound is carbamate-based JZL184 described by Long et al.[35]

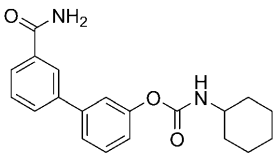

URB597

To date, five X-ray crystal structures of FAAH have been reported.[26d,36,37] Conversely, to the best of our knowledge, there are as yet no publicly available X-ray crystal structures of

[a] *H. Käsnänen,[+] A. Minkkilä,[+] Dr. S. M. Saario, Dr. T. Nevalainen, Prof. Dr. A. Poso*
Department of Pharmaceutical Chemistry, University of Kuopio
P.O.Box 1627, 70211 Kuopio (Finland)
Fax: (+358) 17-162-456
E-mail: antti.poso@uku.fi

[b] *M. J. Myllymäki,[+] A. O. Kataja, Prof. Dr. A. M. P. Koskinen*
Department of Chemistry, Helsinki University of Technology
P.O.Box 6100, 02015 TKK (Finland)

[c] *H. Käsnänen[+]*
Division of Pharmaceutical Chemistry and Centre for Drug Research
University of Helsinki, P.O.Box 56, 00014 University of Helsinki (Finland)

[d] *Dr. S. M. Saario*
The Skaggs Institute for Chemical Biology and Department of Chemical Physiology, The Scripps Research Institute
10550 North Torrey Pines Road, La Jolla, California 92037 (USA)

[+] These authors contributed equally.

Supporting information for this article is available on the WWW under http://dx.doi.org/10.1002/chem.200900390.

MGL[38] (although homology models have been described).[34,39] Consequently, structure-based computational methods have been widely used to study the binding site properties,[20,40,41] the catalytic mechanism,[42–44] and inhibition of FAAH.[45,46]

The structure–activity relationships (SAR) of phenyl *N*-alkylcarbamates as FAAH inhibitors have been extensively explored by Piomelli et al.[20,40,47,48] and also by us.[41,49,50] Additionally, statistical modeling, namely quantitative structure–activity relationships (QSAR), has been applied to correlate FAAH inhibition to the molecular features of the carbamates. In particular, Piomelli et al. utilized one- and two-dimensional descriptors to create classical QSAR models.[20,40,48] Moreover, they have studied the chemical substitutions of the *O*-aryl moiety with comparative molecular similarity indices analysis (CoMSIA), a well-established 3D-QSAR method.[47] However, thus far, no externally validated public 3D-QSAR models of carbamates as FAAH inhibitors have been presented, even though this is a well-studied FAAH inhibitor class.

Herein, we report the design and synthesis of 37 novel *O*-phenyl carbamates with various polar groups at the *meta*-position of the phenyl ring (**1b**–**12**) and their inhibition potencies against FAAH, as previously described.[29] The compounds were designed as inhibitors of FAAH, but all of them were also screened against MGL in order to gain information about their selectivity.[51] In addition, we combined the inhibition data of the present compounds (**1**–**12**, Table 1) to those of our previously reported carbamates (**43**–**108**, Table 2),[41,49,50] and developed CoMSIA[52] and GRID/GOLPE 3D-QSAR models using docking-based alignments. A total of 99 carbamates, divided into training and test sets, were used for model building and validation, respectively.

Previously we found that a 1,2,3-thiadiazol-4-yl group at the *meta*-position of *O*-phenyl carbamates was highly favorable for FAAH inhibition (**1a**, IC_{50} = 240 pM).[49] Thus, thiadiazole was selected as a *meta*-substituent of the phenyl ring (compounds **1a**–**f**) to establish the optimal *N*-alkyl group for FAAH inhibition. Moreover, owing to our previous finding that 3-(4,5-dihydrooxazolyl)phenyl *N*-cyclohexylcarbamate was an extremely potent FAAH inhibitor (IC_{50} = 1.2 nM),[41] a 2-oxazole moiety (**2a**–**d**) was selected as another approach to assess the optimal *N*-group. An *N*-dodecyl group was excluded from our selection since the aim was to avoid compounds with excessive lipophilicity, although several studies have shown that when increasing the lipophilicity of the carbamate, the in vitro inhibitory activity of the compound increases.[50] However, in vivo it is likely to pose problems, such as low solubility and reduced bioavailability. Finally, we prepared carbamates **3**–**12** with either *N*-cyclohexyl or *N*-cyclopentyl moieties, to study the effect of different polar groups at the *meta*-position of the phenyl ring.

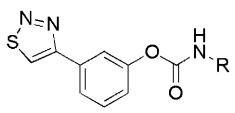

1a; R= *n*-dodecyl[49]
b; R= cyclohexyl
c; R= cyclopentyl
d; R= benzyl
e; R= phenyl
f; R= isopropyl
g; R= hexyl
h; R= 4-phenylbutyl

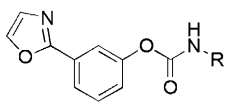

2a; R= cyclohexyl
b; R= cyclopentyl
c; R= 2-methylbenzyl
d; R= phenethyl

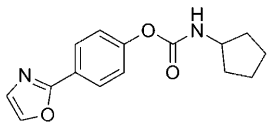

3

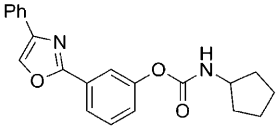

4

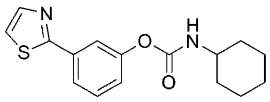

5

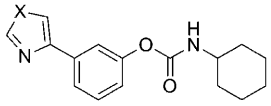

6a; X= O
b; X= NCONHcyclohexyl
c; X= NH
d; X= NMe

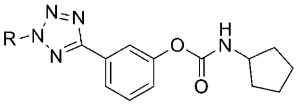

7a; R= H
b; R= Me
c; R= Bn

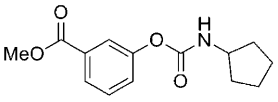

8

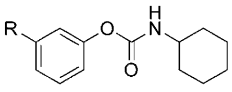

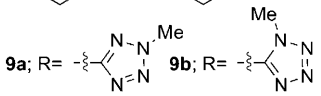

9a; R=

9b; R=

9c; R= CO_2Me
d; R= CO_2H
e; R= CN
f; R= $CONH_2$
g; R= CHO

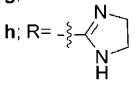

h; R=

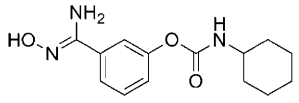

10

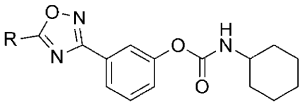

11a; R= Me
b; R= 2-cyclopentylethyl
c; R= *t*Bu
d; R= *n*Bu
e; R= CO_2Et

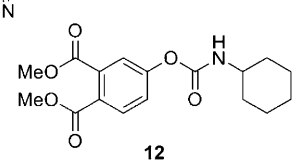

12

Results and Discussion

Chemistry

Most of the carbamates (**1b**–**12**) were prepared by coupling various substituted phenols with suitable isocyanates. The reactions were carried out in the presence of a catalytic amount of triethylamine in toluene at room temperature or reflux. Various methods were used to prepare the phenols that were not commercially available (Scheme 1–5).

The 1,2,3-thiadiazol-4-yl-containing phenol **15**, used to prepare carbamates **1b**–**h**, was formed from phenyl ketone **13** by

the Hurd–Mori reaction via hydrazones **14**, as described previously.[53,54] The 2-oxazole and 2-thiazole moieties for phenols **18a–c** and **21**, used to prepare carbamates **2a–5**, were synthesized using the modified Bredereck method, followed by the demethylation of phenyl ethers using ionic liquid under microwave irradiation (Scheme 1).[55,56]

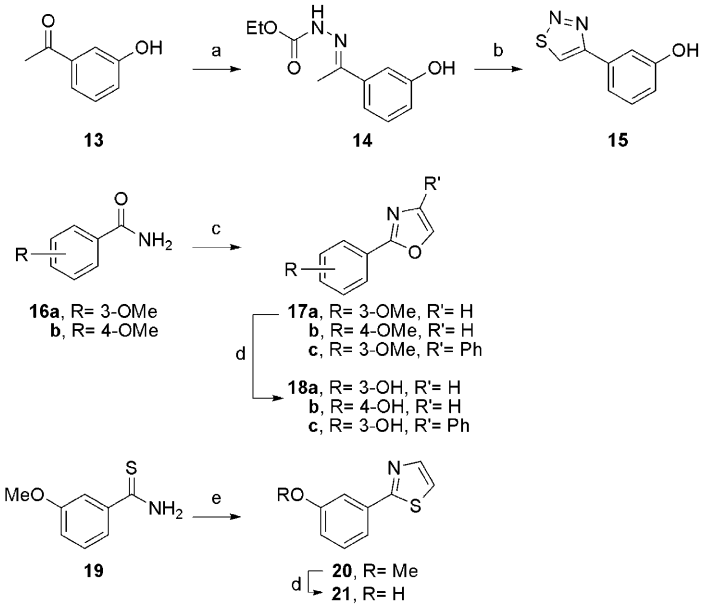

Scheme 1. *Reagents and conditions*: a) Ethylcarbazate, *p*-TsOH, toluene, reflux, 69%; b) $SOCl_2$, RT, 71%.; c) 2-Bromoacetaldehyde diethyl acetal, neat, MW, 45–79%; d) 1-Butyl-3-methylimidazolium bromide or *N*-butylpyridinium bromide, MW, 60–65%; e) 2-Bromoacetaldehyde diethyl acetal, THF, MW, 42%.

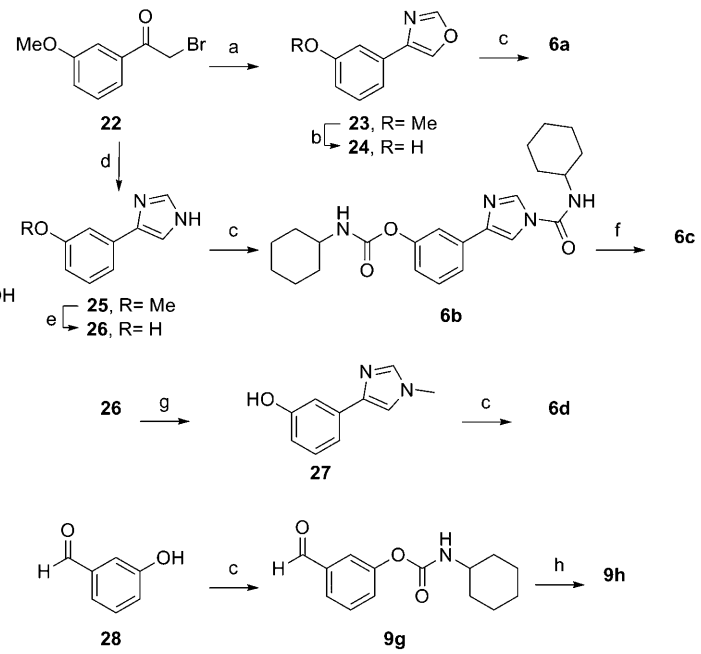

Scheme 2. *Reagents and conditions*: a) Formamide, MW, 100 °C, 51%; b) 1-Butylpyridinimium bromide, MW, 100 °C, 56%; c) Et_3N, RNCO, toluene, reflux, 43–90%; d) Formamide, 165 °C, 85%; e) BBr_3, CH_2Cl_2, −78 °C→RT, 80%; f) NaOH, CH_3OH, CH_2Cl_2, RT, 71%; g) MeI, DMF, 0 °C→RT, 48%; h) Ethane-1,2-diamine, NBS, CH_2Cl_2, −2 °C→RT, 85%.

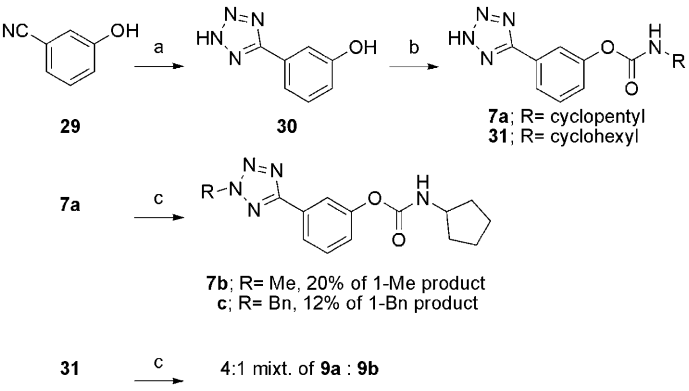

Scheme 3. *Reagents and conditions*: a) NaN_3, Et_3NHCl, toluene, reflux, 85%; b) Et_3N, RNCO, toluene, reflux, 80%; c) MeI, Et_3N, acetone, 2 °C, 44%; or BnBr, KI, Et_3N, acetone, 2 °C, 60%.

The 4-oxazole- (**24**) and 4-imidazole- (**26**) containing phenols were prepared in a similar to 2-oxazoles; heating of bromoketone **22** and an excess of formamide under MW irradiation (for oxazole) or in an oil bath (for imidazole), followed by demethylation of aryl ethers **23** and **25**. In some cases the coupling of isocyanate and phenol as the last step proved difficult. Thus, compound **6c** was prepared via selective hydrolysis of **6b**, since the nitrogen of the imidazole is more nucleophilic than the oxygen of the phenol. Similarly, compound **9h** was prepared by first making the cyclohexylcarbamate of 3-hydroxybenzaldehyde (**9g**) and then converting the aldehyde group to the imidazoline (Scheme 2).[57]

Carbamates **7a** and **31** were prepared by converting nitrile **29** to tetrazole **30**,[58] which was then coupled with either cyclopentyl or cyclohexyl isocyanate. Compounds **7b–c** and **9a–b** were prepared from **7a** and **31** by alkylation of the tetrazole ring. In the methylation of tetrazole the isomeric ratio was 4:1 for less hindered 2-position (**7b** and **9a**). In the benzylation reaction for the preparation of **7c**, similar trend to the methylation reaction was observed, albeit with the ratio 8:1 for the 2-isomer. The 1-substituted methyltetrazole **9b** was isolated from the mixture of isomers by flash chromatography (Scheme 3).

Compounds **11a–e** were prepared by first protecting the phenol functionality of 3-cyanophenol (**29**) as the methoxyethoxymethyl (MEM) ether (**32**), followed by the conversion of the cyano group to amidoxime (**33**). Amidoxime was then converted to various acyl amidoximes (**34a–d**) applying the method described by Unangst et al.[59] The cyclization of acyl amidoximes to 3,5-disubstituted-1,2,4-oxadiazoles (**35a–d**) was performed in the presence of a catalytic amount of TBAF.[60] However, in the preparation of **37** the cyclization occurred without TBAF treatment. Finally, deprotection of the phenolic hydroxy was carried out using $ZnBr_2$ (Scheme 4).[59]

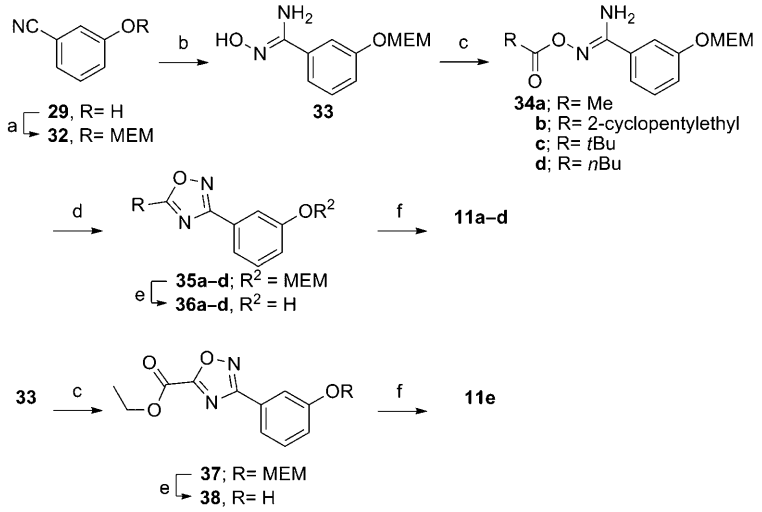

Scheme 4. *Reagents and conditions*: a) Methoxyethoxymethyl chloride, Et_3N, THF, reflux, 88%; b) Hydroxylamine hydrochloride, Et_3N, EtOH, RT, 77%; c) Acetyl-/cyclopentylpropionyl-/trimethylacetyl- or pentanoyl chloride or ethyl chlorooxoacetate, Et_3N, $CHCl_3$, RT, 30–68%; d) TBAF, THF, RT, 81–100%; e) $ZnBr_2$, CH_2Cl_2, RT, 24–49%; f) Cyclohexylisocyanate, Et_3N, toluene, RT, 95%.

enzymatic activity of FAAH for compounds **1a**–**12** are presented in Table 1. The FAAH inhibition activities of 1,2,3-thiadiazol-4-yl-substituted compounds **1b**–**d** and **1g**–**h** demonstrate that the carbamate N-group has a minor effect on potencies. However, the *N*-cyclohexyl substituent (**1b**) was found to be the most favorable for the FAAH inhibition. Interestingly, introduction of *N*-phenyl (**1e**) and *N*-isopropyl (**1f**) groups led to a 10- and 100-fold decrease in inhibition, respectively. This can be due to reduced lipophilic interactions within the active site (**1f**) or the absence of chemical stability (**1e**).[50] Within 2-oxazole containing compounds **2a**–**d**, the inclusion of an *N*-cyclohexyl group (**2a**) was found to give the most potent FAAH inhibitor with an IC_{50} value of 0.74 nM.

After establishing the optimal *N*-alkyl group for FAAH inhibition, we prepared a series of *N*-cyclohexyl (**1b**–**g**) and *N*-cyclopentyl (**2a**–**d**) carbamates with various heterocyclic or acyclic hydrogen-bonding groups. Compounds containing the *N*-cyclohexyl group proved to be the most efficacious FAAH inhibitors. However, we have previously shown that the *N*-cyclopentyl moiety can be as efficacious as the *N*-cyclohexyl group, depending on the *meta*-substituent in the phenyl ring.[50] Therefore, we prepared compounds with *N*-cyclopentyl moieties to study this effect in more detail. Within the *N*-cyclohexyl carbamates, the 2-thiazole containing compound (**5**) had a higher

The preparation of compounds **8**, **9c**–**f**, **10** and **12**, containing small acyclic polar groups at the 3-position of the phenyl ring, is presented in Scheme 5.

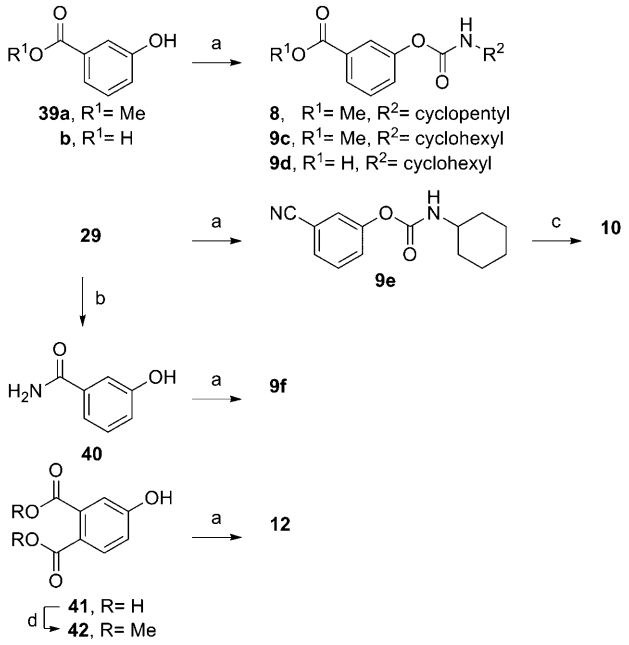

Scheme 5. *Reagents and conditions*: a) Et_3N, RNCO, toluene, reflux, 80–95%; b) $NaBO_3{\cdot}4H_2O$, H_2O, CH_3OH, 54%; c) Hydroxylamine hydrochloride, Et_3N, EtOH, RT, 29%; d) CH_3OH, H_2SO_4, reflux, 98%.

Table 1. IC_{50} and pIC_{50} values for FAAH inhibition by compounds **1a**–**12**.

Compd[a]	IC_{50}[b] [nM]	pIC_{50}	Compd[a]	IC_{50}[b] [nM]	pIC_{50}
1a#[c]	0.24 (0.20–0.30)[c]	9.620	**7a**	21 (18–24)	7.678
1b	1.0 (0.8–1.4)	9.000	**7b**	2.5 (2.0–3.1)	8.602
1c	4.3 (3.2–5.8)	8.367	**7c**	39 (33–45)	7.409
1d	7.4 (5.9–9.2)	8.131	**8**	17 (13–21)	7.770
1e	0%[d]	–	**9a**	1.1 (0.9–1.4)	8.959
1f	70 (47–104)	7.155	**9b**	66 (56–76)	7.180
1g#	1.8 (1.5–2.2)	8.745	**9c**#	3.9 (3.3–4.7)	8.409
1h	3.3 (2.7–4.0)	8.481	**9d**	9%[d]	–
2a	0.74 (0.59–0.92)	9.131	**9e**	49 (42–58)	7.310
2b	5.2 (4.6–5.9)	8.284	**9f**	62 (54–72)	7.208
2c	6.6 (5.0–8.7)	8.180	**9g**	100 (87–120)	7.000
2d	12 (9.5–15.0)	7.924	**9h**	220 (180–250)	6.668
3#	91 (74–113)	7.041	**10**	45%[d]	–
4	0%[d]	–	**11a**	1.6 (1.3–2.1)	8.796
5	5.7 (5.0–6.6)	8.244	**11b**	66 (55–80)	7.180
6a	11 (10–13)	7.959	**11c**	42%[d]	–
6b	43 (37–48)	7.367	**11d**	15 (13–18)	7.824
6c	3.3 (2.8–3.8)	8.481	**11e**	38 (31–47)	7.420
6d	6.9 (5.5–8.7)	8.161	**12**	23 (19–27)	7.638

[a] The test set compounds are marked with a # (see Experimental Section). [b] IC_{50} values represent the mean from three independent experiments performed in duplicate with 95% confidence intervals shown in parentheses. Enzyme activity was completely abolished at the highest tested concentration. [c] See reference [38]. [d] Inhibition [%] at 100 nM. The percentage of inhibition is represented as the mean from two independent experiments performed in duplicates.

FAAH inhibition

All FAAH inhibition data used to derive the 3D-QSAR models (Tables 1 and 2) were obtained under the same experimental conditions in our laboratory.[51] The results of the inhibition of

Table 2. pIC_{50} values for FAAH inhibition by previously published compounds **43**–**103**.[a]

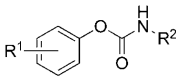

Compd[b]	R^1	R^2	pIC_{50}	Compd[b]	R^1	R^2	pIC_{50}
43	3-(Benzo[*d*]oxazole-2-carbonyl)	Et	6.421	**76**#	4-Thiadiazol-4-yl	*n*Bu	6.796
44#	3-(Benzo[*d*]oxazole-2-carbonyl)	*n*Pr	6.963	**77**#	4-Thiadiazol-4-yl	*n*Hex	7.721
45#	3-(Benzo[*d*]oxazole-2-carbonyl)	*n*Bu	7.268	**78**	4-Thiadiazol-4-yl	dodecyl	7.921
46#	3-(Benzo[*d*]oxazole-2-carbonyl)	*c*-pentyl	7.553	**79**	4-Thiadiazol-4-yl	*c*-pentyl	7.699
47	3-(Benzo[*d*]oxazole-2-carbonyl)	*c*Hex	7.328	**80**	4-Thiadiazol-4-yl	*c*Hex	7.678
48#	3-(Benzo[*d*]oxazole-2-carbonyl)	Bn	6.818	**81**	4-Thiadiazol-4-yl	Bn	7.357
49	3-(Benzo[*d*]oxazole-2-carbonyl)	3-MeBn	7.495	**82**#	4-CO_2Me	*n*Hex	7.509
50#	3-(Benzo[*d*]thiazole-2-carbonyl)	Et	6.623	**83**	4-CO_2Me	dodecyl	7.602
51	3-(Benzo[*d*]thiazole-2-carbonyl)	*n*Pr	6.845	**84**	4-NO_2	*n*Hex	7.569
52#	3-(Benzo[*d*]thiazole-2-carbonyl)	*n*Bu	6.987	**85**	4-CN	*n*Hex	7.886
53#	3-(Benzo[*d*]thiazole-2-carbonyl)	*c*-pentyl	7.328	**86**	4-Br	*n*Hex	7.745
54	3-(Benzo[*d*]thiazole-2-carbonyl)	*c*Hex	7.252	**87**	H	*n*Hex	7.041
55	3-(Benzo[*d*]thiazole-2-carbonyl)	Bn	6.917	**88**#	H	dodecyl	7.036
56#	3-(Benzo[*d*]thiazole-2-carbonyl)	3-MeBn	7.420	**89**	4-(4,5-Dihydrothiazol-2-yl)	Et	5.824
57	4-(Benzo[*d*]oxazole-2-carbonyl)	*c*-pentyl	6.541	**90**#	4-(4,5-Dihydrothiazol-2-yl)	*n*Pr	5.770
58	4-(Benzo[*d*]oxazole-2-carbonyl)	2-MeBn	6.863	**91**	4-(4,5-Dihydrothiazol-2-yl)	*n*Bu	6.284
59	3-Benzo[*d*]-oxadiazol-2-yl	*n*Pr	5.523	**92**#	4-(4,5-Dihydrothiazol-2-yl)	*n*Hex	8.086
60	3-Oxazolo[4,5-*b*]pyridin-2-yl	*n*Pr	6.167	**93**	4-(4,5-Dihydrothiazol-2-yl)	dodecyl	8.201
61	3-Oxazolo[4,5-*d*]pyrimidin-2-yl	*n*Pr	5.347	**94**	4-(4,5-Dihydrothiazol-2-yl)	*t*Bu	5.155
62	3-(4,5-Dihydrooxazol-2-yl)	*n*Pr	7.481	**95**	4-(4,5-Dihydrothiazol-2-yl)	*c*-pentyl	6.886
63#	3-(4,5-Dihydrooxazol-2-yl)	*c*-pentyl	7.886	**96**	4-(4,5-Dihydrothiazol-2-yl)	*c*Hex	7.000
64	3-(4,4-Dimethyl-4,5-dihydrooxazol-2-yl)	*c*-pentyl	7.187	**97**#	4-(4,5-Dihydrothiazol-2-yl)	Bn	6.538
65	3-(*S*)-(4-Methyl-4,5-dihydrooxazol-2-yl)	*c*-pentyl	6.959	**98**	4-(4,5-Dihydrothiazol-2-yl)	2-MeBn	7.208
66	3-(*S*)-(4-Methyl-4,5-dihydrooxazol-2-yl)	*c*Hex	7.292	**99**	4-(4,5-Dihydrothiazol-2-yl)	4-MeBn	6.553
67#	3-(*R*)-(4-Methyl-4,5-dihydrooxazol-2-yl)	*c*Hex	7.796	**100**#	4-(4,5-Dihydrothiazol-2-yl)	4-MeOBn	6.495
68	3-(*S*)-(4-Benzyl-4,5-dihydrooxazol-2-yl)	*c*Hex	5.678	**101**	4-(4,5-Dihydrothiazol-2-yl)	2-PhEt	7.420
69#	3-(*R*)-(4-Benzyl-4,5-dihydrooxazol-2-yl)	*c*Hex	6.229	**102**	4-(4,5-Dihydrooxazol-2-yl)	*n*Bu	6.921
70	3-(*R*)-(4-Methoxycarbonyl-4,5-dihydrooxazol-2-yl)	*c*Hex	7.046	**103**	4-(4,5-Dihydrooxazol-2-yl)	*c*-pentyl	7.000
71#	3-(*S*)-(4-Methoxycarbonyl-4,5-dihydrooxazol-2-yl)	*c*Hex	8.027	**104**	4-(4,5-Dihydrooxazol-2-yl)	2-MeBn	7.469
72	3-(*R*)-(5-Methyl-4,5-dihydrooxazol-2-yl)	*c*Hex	7.137	**105**	4-(4,5-Dihydrooxazol-2-yl)	4-MeBn	6.745
73#	3-(*S*)-(5-Methyl-4,5-dihydrooxazol-2-yl)	*c*Hex	8.167	**106**	2-OMe, 4-CO_2Me	*n*Hex	8.260
74	3-(*S*)-(4-(1*H*-Indol-3-yl)-4,5-dihydrooxazol-2-yl)	*c*Hex	5.721	**107**	2-Me, 4-CO_2Me	*n*Hex	7.260
75	3-Thiadiazol-4-yl	*n*Bu	8.161	**108**	2-Thiadiazol-4-yl	dodecyl	7.301

[a] See reference [50] for compounds **43**–**58**, reference [41] for compounds **59**–**74**, and reference [49] for compounds **75**–**108**. [b] The test set compounds are marked with a # (See Experimental Section).

IC_{50} value (5.2 nM) than the corresponding 2-oxazole derivative (**2a**, IC_{50} = 0.74 nM). Surprisingly, within the series of imidazole containing carbamates (**6b**–**d**), compound **6b**, with a rather bulky *N*-cyclohexylcarboxamide group introduced in the imidazole ring, moderately inhibited FAAH (IC_{50} = 43 nM). Differences in the IC_{50} values between the oxazole containing derivative **6a** (IC_{50} = 11 nM) and the imidazole containing compounds **6c** and **6d** (IC_{50} = 3.3 nM and 6.9 nM, respectively) were small. Within the compounds containing polar acyclic substituents at the *meta*-position of the phenyl ring (**9c**–**g**), the compound with a methoxycarbonyl group (**9c**) was the most potent (IC_{50} = 3.9 nM). Carboxylic acid **9d** was the least active derivative, probably due to it being fully ionized at the pH of the in vitro FAAH assay. Imidazoline **9h** gave low inhibition activity compared to the corresponding oxazoline derivative reported in our previous study (IC_{50} = 1.2 nM).[41] The oxadiazole moiety containing compounds **11a**–**e** gave further information about the effect of steric bulk at the heterocyclic moiety; a clear drop in inhibition was observed as the steric hindrance at 5-position in the heterocycle was increased (Me < *n*Bu < CO_2Et < 2-cyclopentyl-ethyl < *t*Bu; inhibition ranged from IC_{50} = 1.6 nM to 42% inhibition at 100 nM).

In addition to *N*-cyclohexyl carbamates, we prepared a series of *N*-cyclopentyl carbamates with 5-tetrazolyl and methoxycarbonyl substituents in the phenyl ring. The presence of a benzyl group as the 2-substituent in tetrazole (**7c**) did not notably decrease FAAH inhibition. The unsubstituted tetrazole **7a** most likely exists in an ionized form at physiological pH, which may affect its inhibition activity, thus explaining the activity difference between **7a** and **7b**. FAAH inhibition by tetrazolyl phenyls **7a**–**c** and **9a**–**b** suggested that the position of the tetrazole substituent (**9a** vs **9b**) was as an important factor as the size of the group (**7b** vs **7c**). With tetrazole groups, in contrast to other compounds in this study, the replacement of *N*-cyclohexyl to *N*-cyclopentyl group did not notably affect the inhibitory potencies, but followed the same trend.

All the compounds were generally selective towards FAAH (see Supporting Information for MGL inhibition, table S1). However, compounds **1g**, **9e**, and **12** were found to inhibit MGL with IC_{50} values in the micromolar range (IC_{50} = 12–34 μM).

Interestingly, compound **3** did not inhibit MGL activity (only 8% inhibition was observed at 1 μM), although we have previously shown that *para*-substitution in phenyl carbamates favors the MGL inhibition.[49,50]

In silico chemical reactivity

There are presumably two main factors governing the FAAH activity of the carbamates: firstly, the susceptibility of the ligands to react with the enzyme, and secondly, the steric and electric complementarity of the carbamates and FAAH. Irreversible inhibition of FAAH by URB597[20] and related compounds,[46,61] is known to involve carbamoylation of the hydroxy group of the catalytic Ser241 residue. Furthermore, the carbamate C(O)–O bond lability and the pK_a value of the phenoxide leaving group has been used to explain the variance in biological activity.[62,63] On the other hand, there are several examples of carbamate design suggesting that molecular recognition interactions account for the majority of the variance in the FAAH inhibition data.[40–42] Thus, prior to building any 3D-QSAR models we needed to evaluate whether there were actual prerequisites to correlate the inhibition activity with noncovalent enzyme–ligand (recognition) interactions by assessing the degree of correlation between the FAAH IC_{50} values of the compounds and the calculated reactivity. To achieve this, we plotted quantum chemical energies of the highest occupied molecular orbital (E_{HOMO}) and the lowest unoccupied molecular orbital (E_{LUMO}), and the calculated chemical hardness (η) against the pIC_{50} values of the full data set. Of the calculated descriptors, E_{LUMO} was able to explain 13% of the variance in the data, while E_{HOMO} and chemical hardness were even less significant (Table 3; a full list of calculated values is given in table S3 of the Supporting Information).

Table 3. Linear regression models of FAAH inhibition.

Equation	n[a]	r^2[b]	S[c]	F
$pIC_{50} = 2.88E_{HOMO}$[d] $+8.31$	99	0.002	0.842	0.223
$pIC_{50} = 4.32E_{LUMO}$[e] $+7.01$	99	0.130	0.837	1.278
$pIC_{50} = 6.26\eta$[f] $+6.09$	99	0.007	0.804	0.677

[a] The linear regression models were calculated with the full data set. [b] Conventional, nonvalidated correlation coefficient. [c] Standard error of estimate. [d] The calculated energy of the highest occupied molecular orbital (HOMO). [e] The calculated energy of the lowest unoccupied molecular orbital (LUMO). [f] The calculated estimate of chemical hardness.

According to the frontier molecular orbital (FMO) theory, molecules with near-zero E_{HOMO} are good nucleophiles while those with low E_{LUMO} are good electrophiles.[64] Chemical hardness is a measure of the resistance of the compound to deformation with high values implying high chemical stability.[65] Although these are simple descriptors, they have been successfully applied in carbamate-related quantitative structure–property relationships (QSPR) studies.[40,63] While it is likely that higher correlation coefficients with FAAH pIC_{50} values could be found by dividing our data set in more specific substructural families, we can assume, based on the results presented in Table 3, that in general the level the reactivity of the compounds has a minor effect and is unable to explain the large observed variance in FAAH inhibition in our data set (Table 1 and Table 2).

Training and test set selection

Rational selection of training and test sets in terms of representativeness and diversity can be seen as a general requirement when applying external validation in QSAR studies.[66] For any prediction to be valid, the predicted set of compounds must fall within the same chemical space as the training set compounds (i.e., possess similar chemical properties). There are several methods to select the sets, such as random selection, sorted activity data, and *k*-means clustering, of which the latter is argued to be superior to the others.[67] We divided our data (99 carbamates) into training and test sets of 74 and 25 carbamates, respectively, using two-dimensional fingerprint-based *k*-means clustering (Tables 1 and 2). The FAAH pIC_{50} value distributions of the sets were compared and found statistically equal (independent two-sample *t*-test; $t(97) = 0.18$, $p < 0.001$; $M_{Training} = 7.36$, $SD = 0.88$, $n = 74$; $M_{Test} = 7.39$, $SD = 0.85$, $n = 25$). The distribution of the sets in molecular operating environment (MOE) two-dimensional descriptor space, as evaluated by principal component analysis (PCA), is presented in Figure 1, which shows the sets are uniformly spread over the first two dimensions of the PCA space, and are representative of each other. On the other hand, both sets are also diverse within the defined space. Compound **88** can be regarded as an outlier, and consequently, possibly more inaccurately predicted by the 3D-QSAR models.

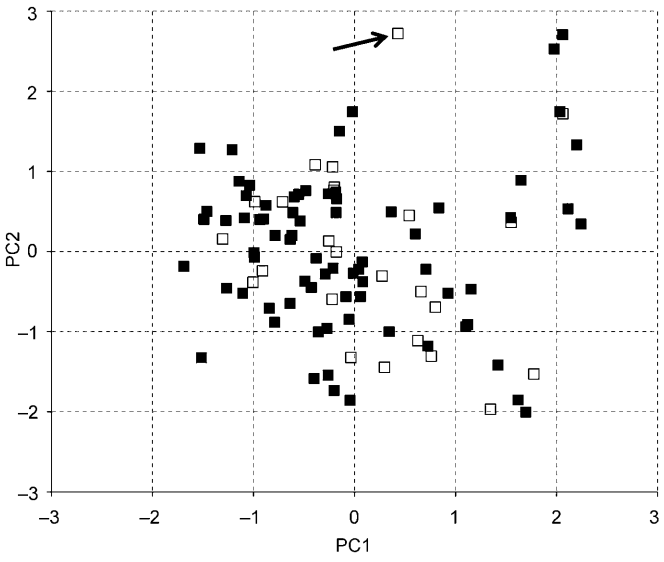

Figure 1. Two-dimensional plot of the first two principal components (PCs) of MOE PC analysis (test set compounds, □; training set compounds, ■). The first (PC1) and the second (PC2) PCs accounted for 30.9% and 15.8% of the variance in the data, respectively. The arrow is highlighting compound **88**.

Alignment by molecular docking

The superposition of the compounds is known to be one of the most crucial steps in any 3D-QSAR study. Herein, we used the available structural FAAH data in protein-based alignment by molecular docking. This enables direct projection of the resulting 3D-QSAR contours into the enzyme active site, and furthermore, the usage of the ligand-based QSAR data in later structure-based design. Although X-ray structures of humanized rat FAAH (h/rFAAH) have recently become available (PDB: 2WAP, 2VYA, 2WJ1, 2WJ2),[26d,37] owing to the enzyme source (rat) used in our in vitro biological evaluation of these compounds, we chose to exploit the first publicly available murine FAAH crystal structure (PDB: 1MT5) in our docking experiments.[36]

The first hypothesis of the FAAH binding orientation of URB597 and its derivatives placed the *O*-aryl moiety into the opening of the acyl chain binding (ACB) channel, mimicking the lipophilic alkyl chain of methyl arachidonyl fluorophosphonate (MAFP), the substrate found in the co-crystal X-ray structure (PDB: 1MT5).[20] However, according to more recent studies,[41,46,48,62] prior to the carbamoylation reaction, carbamates bind in a conformation where the *N*-alkyl group is pointing towards the bifurcated ACB and substrate-access channels, while the carbonyl oxygen is interacting with the oxyanion hole residues (Ile 238–Ser 241) with the electropositive α-carbon of the ligand in close proximity to the Ser 241 hydroxy group. Moreover, in this binding mode, the *O*-aryl group resides in the cytoplasmic access (CA) cavity.

The molecular mechanistic docking scheme cannot take into account the proton transfer in the FAAH Lys 142–Ser 217–Ser 241 catalytic triad,[68,69] the high electropositivity of the oxyanion hole,[37b] nor the polarization in the ligand carbamate functionality. Thus the energy surface of the protein–ligand interactions in the catalytic region is likely to be ill defined. In order to produce consistent alignments in agreement with the binding mode described above, Surflex-Dock™ (Tripos, Ltd., St. Louis, USA) was used in the fragment-guided mode.[70] First, we explored the effect of varying the penalty value in the fragment-guided docking scheme. The docking runs were evaluated by the CoMSIA partial least squares (PLS) statistical parameters. Figure 2 shows that in terms of external (test set) predictivity, the most dramatic effect is observed when the penalty value is increased from 0 to 1 pK_d Å^{-2}. No clear trend in statistical values is apparent when the penalty value is further increased to the maximum value of 100 pK_d Å^{-2}. Although slightly better models could be built with larger penalties (more constrained alignments), we chose to use as small value as possible, allowing the ligands to adjust their conformations also according to the enzyme–ligand interactions rather than solely the predefined fragment position. Therefore, subsequent 3D-QSAR models were developed using the best-ranked conformations of each ligand from the docking with penalty value of 1 pK_d Å^{-2} (both with and without the post-docking minimization, see Figure 3 and Supporting Information, figure S2).

Interestingly, in the chosen alignments, the *N*-cyclohexyl moiety of carbamates (e.g., **2a**) adopts a conformation where

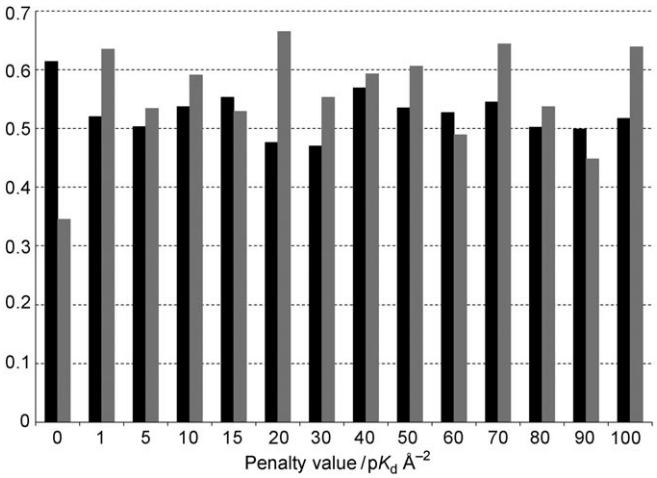

Figure 2. Evaluation of Surflex-Dock™ fragment guiding penalty values in ligand alignments (q^2_{SAMPLS}, ■; r^2, ■). The statistical values shown are for CoMSIA models using Gasteiger–Hückel charge model and the combination of all five CoMSIA descriptors (steric, electrostatic, hydrophobic, hydrogen bond donor and acceptor). Post-docking minimization was employed in the docking process (see Experimental Section). The corresponding values for a model without any fragment guiding in the docking process were: $q^2_{SAMPLS} = -0.042$, $r^2 = 0.342$, and $R^2_{PRED} = 0.252$. See table S4 in the Supporting Information for full statistical parameters of the models.

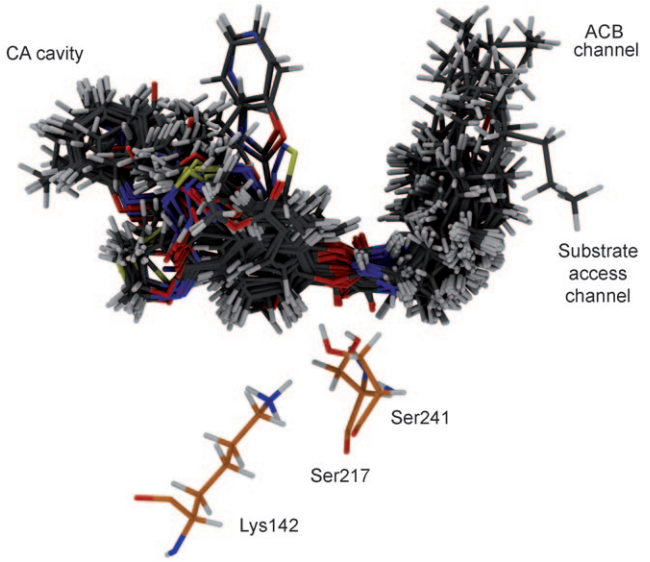

Figure 3. The FAAH active site-based alignment of the 99 carbamates by Surflex-Dock™ with a penalty value of 1 pK_d Å^{-2} (no post-dock minimization). The carbon atoms of the catalytic residues are colored in orange, while those of ligands in grey.

the carbamate group is in an axial position (Figure 5 and 6, see also Supporting Information, figure S4 and S5). The side chains of Phe 194 and Ile 491 sterically prevent the cyclohexyl ring from binding with carbamate in an equatorial position. Similar observations were also made in our earlier study.[41] This is in disagreement with the previous studies by Piomelli et al.,[20,40,48] which were performed using the same X-ray struc-

ture of FAAH. This discrepancy is peculiar, and might originate from the differences in the applied docking and geometry optimization schemes. However, conformational analysis and quantum mechanical calculations of compound **2a** (see Supporting Information) suggest that the *N*-cyclohexyl conformation, with carbamate group in the axial position, is a plausible initial binding conformation for these inhibitors.

CoMSIA models

Descriptor selection

By default, CoMSIA uses five descriptor types: steric, electrostatic, hydrophobic, hydrogen bond donor and acceptor.[52] Typically, all of these are applied in standard CoMSIA analyses. However, the number of descriptors selected for QSAR models should be kept to a minimum.[71] To find the most (internally) predictive field combination prior to actual model building, preliminary q^2 values were calculated with the SAMPLS[72] algorithm for all 31 descriptor field combinations. The combination of steric, electrostatic, and hydrophobic descriptors gave rise to the highest q^2 values, although not by a significant margin (see Supporting Information, figure S3.) Additional progressive scrambling analyses confirmed this combination as having the highest internal predictivity (data not shown), and thus the combination was used in the subsequent model development.

Table 4. Statistics of CoMSIA PLS analyses.[a]

Model[b]	cv[c]	q^{2}[d]	S_{PRESS}[e]	N[f]	r^{2}[g]	S[h]
Minimized						
GH	LHO	0.380	0.669	2	0.696	0.491
	LOO	0.594	0.584	6	0.893	0.299
MNDO	LHO	0.411	0.680	2	0.709	0.480
	LOO	0.563	0.605	6	0.895	0.297
ESP	LHO	0.453	0.661	3	0.775	0.425
	LOO	0.566	0.603	6	0.898	0.292
Non-minimized						
GH	LHO	0.368	0.724	6	–[i]	–
	LOO	0.580	0.593	6	0.906	0.281
MNDO	LHO	0.417	0.681	3	0.784	0.416
	LOO	0.593	0.584	6	0.910	0.274
ESP	LHO	0.408	0.688	3	0.781	0.419
	LOO	0.592	0.585	6	0.913	0.269

[a] pIC_{50} value of FAAH inhibition was used as a dependent value for the set of 74 carbamate derivatives. Steric, electrostatic, and hydrophobic CoMSIA descriptors were used. [b] Alignments with a penalty value $=1$ pK_d Å^{-2} both with and without the post-docking minimization. Charges calculated with Gasteiger–Hückel (GH), semiempirical modified neglect of differential overlap (MNDO), and HF/6-311G** electrostatic potential fit (ESP) methods. [c] Cross-validation method. Column filtering of 0.001 kcal mol^{-1} was applied. [d] Cross-validated correlation coefficient. [e] Standard error of prediction. [f] Number of PLS components. [g] Conventional, nonvalidated correlation coefficient. [h] Standard error of estimate. [i] Determined below.

Statistical results

CoMSIA models were derived for the docking alignments (penalty value $=1$ pK_d Å^{-2}) both with and without the post-docking geometry optimization. Three different partial-charge models were applied for both alignments. The results of the CoMSIA models are summarized in Table 4. In terms of the popular criterion of $q^2_{LOO} > 0.5$, though highly controversial due to its often overly optimistic results,[73,74] both alignments could produce statistically significant models with all the charge models. Additionally, much stricter leave-half-out (LHO) cross-validation was also performed. Compared to leave-one-out (LOO) cross-validation, LHO resulted in clearly lower q^2 values throughout the models (0.566–0.594 vs 0.368–0.453, respectively), casting a shadow on the quality of the models. Also, it should be noted that the large gap between q^2 and r^2 in the CoMSIA models might be due to meaningless X-variables (descriptor values), suggesting that the models contain noise. The field contributions of the nonvalidated models are presented in Supporting Information (table S5). The electrostatic and hydrophobic fields had the highest contribution to the models (39–44% and 30–40%, respectively).

The models with electrostatic-potential- (ESP) fitted charges were higher in internal predictivity compared to those with topological Gasteiger–Hückel (GH) or semiempirical modified neglect of differential overlap (MNDO) charges. The partial charge calculation method reportedly influences comparative molecular field analysis (CoMFA)[75] and CoMSIA[76] models with more sophisticated methods resulting in more predictive models. In the present study, the better internal predictivity of ESP charges was already seen in the descriptor selection (Supporting Information, figure S3), and it is likely to result from the applied ab initio method taking into account the polarized electron distribution of the carbamates more precisely than the other charge calculation methods. However, it should noted that ESP-derived charges are prone to be less accurate in determination of charges of "buried" atoms, such as sp^3 carbon, as the ESP points used in fitting are relatively far away from these atoms.[77]

Region focusing

The models in Table 4 were subjected to region focusing[78] in order to refine the models. The results for all the focused models are given in the Supporting Information (table S6) while the statistics of the focusing of the model with non-minimized alignment (ESP charges) are presented in Table 5. Generally, compared to the parent models, region focusing clearly increased the internal predictivity. The highest values for all the models were observed with grid spacing of 1.0 Å (for comparison, the default value of 2.0 Å was used in the parent models). As evident in Table 5, focusing simplified the model, as only five components were needed for the best results (compared to six components in the original models). Applying a finer grid (0.5 Å) did not enhance the results, even with high values of column filtering (data not shown). This might be due to insufficient X-variable selection and filtering protocols in SYBYL, as the small grid spacing value produces large amounts of variable values. The best focused model (non-minimized, ESP charges, grid $=1.0$ Å, weight $=0.5$) was selected for subsequent

Table 5. CoMSIA Region focusing results for the model with non-minimized alignment with ESP-fitted charges.

Weight[a]	w = 0.3		w = 0.5		w = 0.8	
Grid[b]	0.5	1.0	0.5	1.0	0.5	1.0
q^2_{SAMPLS}[c]	0.655	0.694	0.68	**0.710**	0.683	0.701
S_{PRESS}[d]	0.538	0.508	0.538	**0.498**	0.516	0.511
N[e]	6	5	6	**5**	6	6
r^{2}[f]	0.904	0.897	0.903	**0.859**	0.862	0.864
S[g]	0.283	0.294	0.286	**0.341**	0.340	0.338

[a] Weighting value in StDev*Coefficient for each lattice point. [b] Grid spacing in Å. [c] Cross-validated correlation coefficient. SAMPLS equal to leave-one-out with column filtering set to 0 kcal mol^{-1}. [d] Standard error of prediction. [e] Number of PLS components. [f] Conventional, nonvalidated correlation coefficient. Column filtering value of 0.001 kcal mol^{-1} was used for the nonvalidated models. [g] Standard error of estimate.

Table 6. Progressive scrambling statistics.[a]

Model	N[b]	Q_s^{*2}[c]	Q_0^{*2}[d]	SDEP$_s$*[e]	dq^2/dr_{yy}^{2}[f]
Minimized					
GH	5	0.502 ± 0.003	0.591 ± 0.003	0.640 ± 0.002	1.045 ± 0.032
	6	0.515 ± 0.003	0.606 ± 0.003	0.636 ± 0.001	1.077 ± 0.029
Best	4	0.584 ± 0.003	0.687 ± 0.003	0.581 ± 0.002	0.894 ± 0.026
focused[g]	5	0.610 ± 0.000	0.712 ± 0.003	0.569 ± 0.001	1.063 ± 0.024

[a] Values are represented as mean ± standard deviation (SD) of 20 scrambling runs each with 100 scramblings. [b] Number of PLS components. [c] Predictivity at the critical threshold level of perturbation (s); s = 0.85. [d] $Q_0^{*2} = Q_s^{*2}$s, corresponding to the value expected for an unperturbed model (classical q^2). [e] Standard error of prediction at the critical level of perturbation. [f] Sensitivity for perturbation at the critical level of perturbation. [g] Non-minimized alignment, ESP charges, weighting value of 0.5, and grid spacing of 1.0 Å.

studies. The LHO cross-validation q^2 and S_{press} values for this model were 0.563 and 0.599, respectively. Compared to the parent model, the best focused model shows a decrease in the hydrophobic contribution (Supporting Information, table S5). Moreover, the small increase in steric and electrostatic contributions indicates that the model is more sensitive to these effects, although a hydrophobic field still has a significant contribution to the model (30%).

Progressive scrambling

The models were validated internally by progressive scrambling, which can address the overly optimistic cross-validation results by randomly perturbing the models in a step-wise manner and measuring the response to perturbation, hence evaluating the stability and the robustness of the models.[79] The predictivity of redundant models with chance correlations is expected to fall off rapidly in the scrambling process, whereas robust models are likely to remain stable. The progressive scrambling procedure was applied to all the models given in Table 4 and also for the best focused model (see Supporting Information, table S7 for full scrambling results). For the majority of the models, the adjusted Q_0^{*2} values were comparable with the unperturbed LOO q^2 values (Table 6). However, when looking at the values for the sensitivity to perturbation (dq^2/dr_{yy}^{2}), the danger of using the classical q^2 as a measure of the model quality becomes apparent.[73,80] In the optimal case, the value for dq^2/dr_{yy}^{2} should be near unity, that is, the predictivity of the model should respond to perturbation linearly, and a value of 1.2 can be used as a limit to determine if the model is unstable.[79] Thus, dq^2/dr_{yy}^{2} can be used to avoid overfitting caused by too many PLS components.[81]

Evidently, the majority of the models (original number of PLS components) with significant q^2 values were clearly unstable ($dq^2/dr_{yy}^{2} \geq 1.2$; Supporting Information, table S7). Even when the models were simplified by reducing the number of components, overfitting was not completely avoided. Thus, we considered only the most predictive and stable models ($Q_0^{*2} > 0.6$, $dq^2/dr_{yy}^{2} < 1.1$) for further studies (Table 6).

Test set correlation validation

The CoMSIA PLS models were subjected to external validation by test set prediction. This is claimed to be the ultimate QSAR model validation method.[73,82] In addition to the coefficients of correlation for the test set prediction (R^2_{PRED}), the models were evaluated according to the methods of Golbraikh and Tropsha (see Supporting Information, table S8).[73,82b] The R^2_{PRED} values ranged from 0.591 to 0.732 with the best focused model having the highest external predictivity. Of the models, all but one (the minimized alignment with GH charges) passed the requirements of Golbraikh and Tropsha. On the other hand, when combining this data with the progressive scrambling results for model stability, the only model fulfilling all these criteria is the best focused model, and therefore this model was chosen to calculate the CoMSIA contour maps described below. The experimental versus predicted plot of the best focused model is presented in Figure 4. No significant outliers can be seen, though the majority of the compounds are clus-

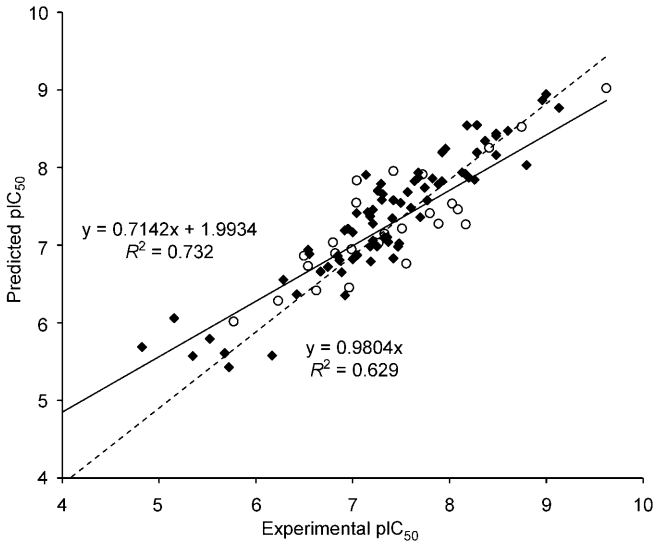

Figure 4. Test set prediction for the best focused, five-component CoMSIA model (training set, ◆; test sets, ○). Best-fit (——, yielding R^2_{PRED}) and zero-intercept (-----, yielding R^2_0) lines and the respective equations are shown.

tered in the center region of pIC_{50} distribution. Naturally, this is due to the data set itself.

CoMSIA fields

Figure 5 shows the CoMSIA steric, electrostatic and hydrophobic contour maps for the best focused model. Field contributions are shown in the Supporting Information (table S5). The steric field (Figure 5 a) shows bulk being favorable in the distal part of the *N*-cyclohexyl group, in the region where the longer alkyl groups are reaching further away from the carbamate core. Additionally, steric bulk is disfavored in the distal *O*-aryl region where the larger substituents are located (e.g., the 2-cyclopentyl-ethyl of **11 b** or the cyclohexyl of **6 b**). Correspondingly, in the FAAH active site, the favored region is in the starting point of the ACB channel with possible interacting amino acids being Leu 192, Phe 194, Ile 491, and Thr 488, whereas the disfavored region almost reaches the hydrophilic surface of FAAH in the CA channel.

In the case of the electrostatic field (Figure 5 b), negative charge is favored in close proximity to polar atoms of the *meta*-heterocycles of the phenyl ring (e.g, the oxazole nitrogen of **2 a** or **6 a**). This is in line with our earlier finding that the oxazoline ring nitrogen interacts with the backbone of Cys 269 and Val 270,[41] although in the present study the ligand conformations are not fully comparable with the earlier work due to the differences in the docking methods. The unfavorable region for negative charge is located in the ketone and phenyl group region of the *meta*-substituted carbamates with large substituents in the distal *O*-aryl tail (e.g., **51**, **55**, **57**). This is controversial, as this ketone group is known to be important for FAAH activity,[41] potentially due to a water-mediated hydrogen bond with Thr 236.[37b] Then again, compared to **2 a**, the phenyl ring of these less potent carbamates is located slightly closer to Leu 192 and Cys 269, and is probably the cause of this disfavored field.

The favorable hydrophobic field (Figure 5 c) highlights the importance of having a five-membered ring in the *meta*-position of the *O*-phenyl group (the carbon or sulfur atoms of the ring are located in this region). Similarly to the steric field, the white hydrophobic field is showing the disadvantage of having lipophilic substituents close to the (hydrophilic) opening of the CA cavity, near the surface of FAAH. The large disfavored region at the *N*-cyclohexyl ring, at the bifurcation point of the ACB and substrate access-channels, does not seem reasonable at first. However, the original CoMSIA atomic hydrophobicity values were fitted from a full molecule property (octanol–water partition coefficient),[52,83] and as a result, for example, the sp^3 carbon of the *N*-cyclohexyl moiety has a negative hydrophobicity value of −0.4873. Consequently, substituents classically considered as hydrophobic can become the opposite, especially due to the inherent Gaussian-type function of CoMSIA calculating the descriptor values inside the van der Waals surface of the molecules. This combined with the large contribution of the hydrophobic field to all the models casts a doubt over the applicability of the current CoMSIA models to rational design of further carbamates as FAAH inhibitors. The

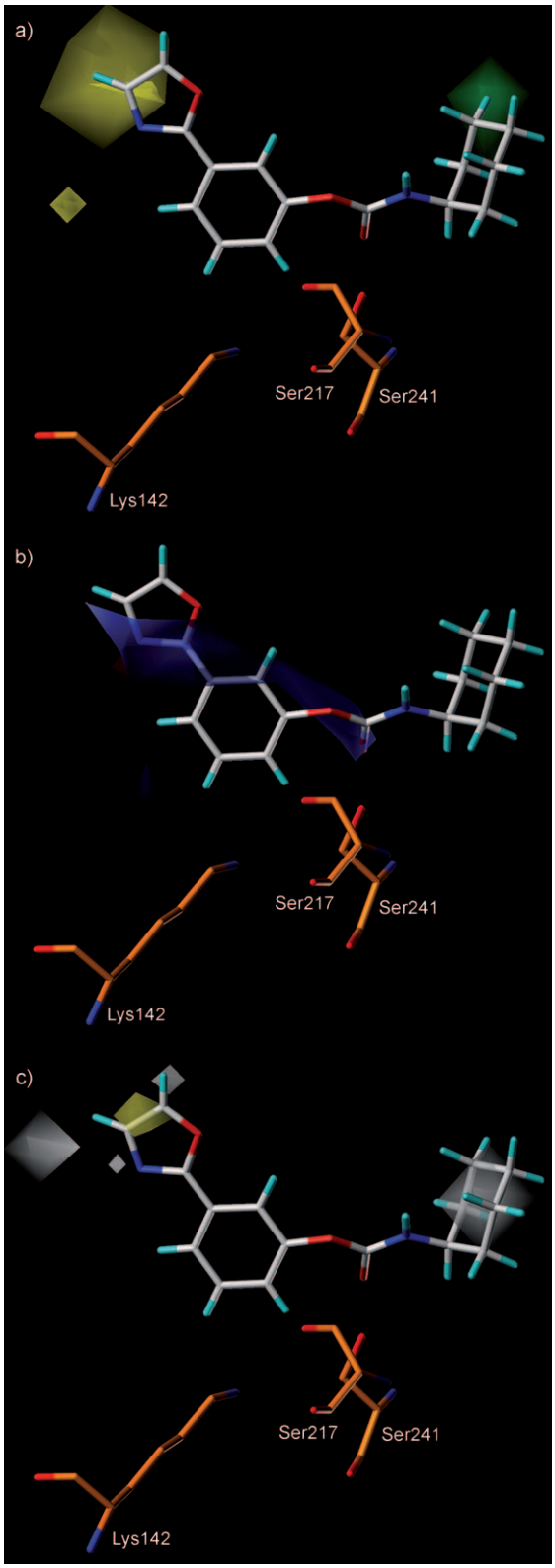

Figure 5. CoMSIA PLS fields (coefficient plots) for the best focused model in the active site of murine FAAH. The most potent carbamate of the training set (**2 a**) is also rendered for the sake of clarity. a) Steric fields: green, bulk favored; yellow, bulk disfavored. b) Electrostatic fields: blue, negative charge disfavored; red, negative charge favored. c) Hydrophobic fields: yellow, hydrophobic groups favored; white, hydrophobic groups disfavored. See figure S4 in the Supporting Information for depiction of the active site surface.

peculiar nature of the CoMSIA hydrophopic descriptor should be investigated further, but it is outside the scope of the current study.

GRID/GOLPE

Owing to the uncertainties in the CoMSIA hydrophobic descriptor described above, we wanted to apply an alternative 3D-QSAR method, that is, the GRID molecular interaction fields combined with GOLPE statistical modeling package to create a QSAR model of FAAH inhibition.[84,85]

Statistical results

Over 60 monoatomic probes (descriptors) are available in GRID (version 22a), and although not all of these are applicable to the current study, we chose not to apply a time-consuming full descriptor selection scheme, but resorted to a common set of probes: steric (sp^3 carbon, C3), and hydrogen-bond donating (amide nitrogen, N1) and accepting (carbonyl oxygen, O) interaction partners. The ligand alignments, and training and test set selections were identical to those of the CoMSIA models, though only a fine grid of 0.5 Å was used for the GRID calculations (corresponding to the smallest value used in CoMSIA region focusing). Following the advanced X-variable pretreatment and selection (see Experimental Section for details), final models were developed (Table 7). The statistical values of the GRID/GOLPE models were clearly better than the nonfocused CoMSIA models (Table 4) with the best GRID/GOLPE model (non-minimized alignment) yielding q^2 and r^2 values of 0.730 and 0.916 at five PLS components, respectively. Noticeably, both models were statistically significant ($q^2 > 0.5$) even when using the strict LHO cross-validation. The GRID/GOLPE models are of a similar level in terms of internal statistics with the final (best focused) CoMSIA model. Unfortunately, the internal robustness and stability could not be studied as progressive scrambling is not available in GOLPE.

Table 7. Statistics of GRID/GOLPE PLS analyses.[a]

Model[b]	cv[c]	q^{2}[d]	S_{PRESS}[e]	N[f]	r^{2}[g]	S[h]
Minimized	LHO	0.516	0.606	5	–[i]	–
	LOO	0.678	0.495	5	0.887	0.299
Non-minimized	LHO	0.531	0.697	5	–[i]	–
	LOO	0.730	0.453	5	0.916	0.253

[a] pIC_{50} value of FAAH inhibition was used as a dependent value for the set of 74 carbamate derivatives. C3, N1, and O GRID probes were used. [b] Alignments with a penalty value $=1$ pK_d Å^{-2} both with and without the post-docking minimization. [c] Cross-validation method. [d] Cross-validated correlation coefficient. [e] Standard error of prediction. [f] Number of PLS components. [g] Conventional, nonvalidated correlation coefficient. [h] Standard error of estimate. [i] Determined below.

Test set correlation validation

Similarly to CoMSIA procedure, GRID/GOLPE models were validated using the external test set. The results are presented in the Supporting Information (table S9). The R^2_{PRED} values for the minimized and non-minimized models were 0.505 and 0.760, respectively. Furthermore, the non-minimized model met the requirements set by Golbraikh and Tropsha,[70,79b] whereas these criteria were not fulfilled in the case of the minimized model. The experimental versus predicted plot of the non-minimized model is presented in Figure 6. In the model test set, compound **72** can be regarded as an outlier (residual value −1.34). Compared to the final CoMSIA model (Figure 4), this model is not as stable; this is also indicated by the mean values of test set absolute residuals (CoMSIA = 0.26, SD = 0.2; GRID/GOLPE = 0.35, SD = 0.28).

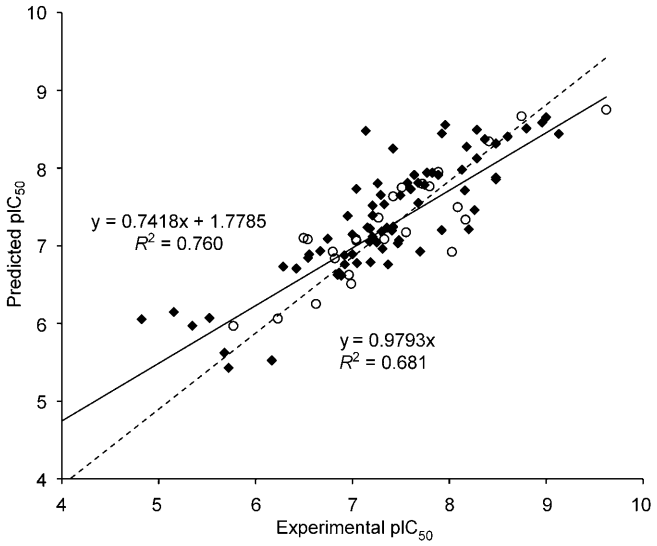

Figure 6. Test set prediction for the five-component, non-minimized GRID/GOLPE model (training set, ◆; test sets, ○). Best-fit (——, yielding R^2_{PRED}) and zero-intercept (-----, yielding R^2_0) lines and the respective equations are shown.

GRID/GOLPE fields

The GOLPE PLS coefficient plots of the non-minimized model are presented in Figure 7. In the case of steric (carbon) probe (Figure 7a) the majority of the favorable regions are located in close proximity to the side chains of Ile 238 and Leu 278, next to the hydrophilic end of the CA channel. This is in line with the earlier results, and highlights the importance of having the carbamate *O*-phenyl ring substitution at the *meta*-position.[40,49,50] These studies have also shown *ortho*- and *para*-substitutions to be suboptimal for FAAH activity. Correspondingly, the unfavorable steric contour shows regions next to Leu 266 and Gly 268 (*para*-substitutions) and Leu 192 (*ortho*-substitutions). Notably, small substituents at the *para*-position are known to be sterically tolerated, decreasing the FAAH activity only by to a small degree.[40,86] Additionally, the carbon probe reflects the shape of the FAAH active site in the branching zone of the ACB and substrate-access channels with disfavored regions being located around the *N*-alkyl/aryl tail of the carbamates. As expected, according to the SAR presented above (e.g., **2a**–**d**), cyclic and acyclic *N*-alkyl groups do not reside in

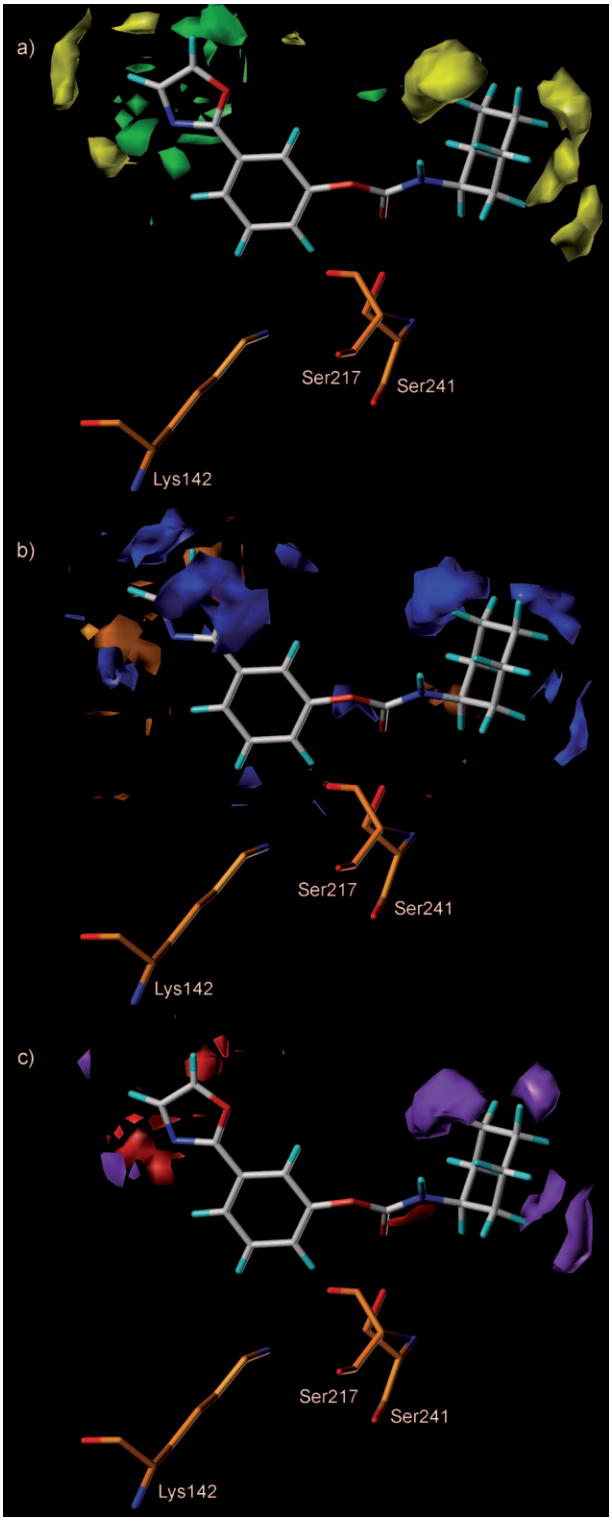

Figure 7. GRID/GOLPE PLS fields (coefficient plots) for the final model in the active site of murine FAAH. The most potent carbamate of the training set (**2a**) is also rendered for the sake of clarity. a) Carbon (C3) fields: green, steric interaction favored (negative coefficients under −0.0005); yellow, steric interactions disfavored (positive coefficients over 0.0005). b) Amide nitrogen (N1) fields: orange, interaction with hydrogen-bond acceptor favored (negative coefficients under −0.0007); blue, interaction with hydrogen-bond acceptor disfavored (positive coefficients over 0.0007). c) Carbonyl oxygen (O) fields: red, interaction with hydrogen-bond donor favored (negative under coefficients −0.0005); violet, interaction with hydrogen-bond donor disfavored (positive coefficients over 0.0005). See figure S5 in the Supporting Information for depiction of the active site surface.

these disfavored regions unlike the more rigid aromatic groups. In the FAAH active site, the side chains of Leu 192, Phe 194 and Ile 491 in particular are sterically constraining the conformation of the *N*-alkyl/aryl groups. However, with urea type FAAH inhibitors, a major increase in inhibition activity was gained by introduction of a biaryl ether moiety, which was shown to interact with the ACB channel in h/rFAAH.[26d,37a] Moreover, h/rFAAH is known to undergo significant conformational changes in the ACB/substrate-access channel region.[26d,37] Thus, the preference for nonaromatic N-substitutions might not be as clear with other in vitro bioassays as in the current study.

The PLS contour of the probe used to account for hydrogen-bond accepting properties (N1) shows two main favorable regions (Figure 7b). These regions are located next to the *meta*-substituents of the *O*-phenyl ring, close to the side chains of Gln 273 and Leu 278. This highlights the importance of having a heterocyclic group capable of forming electrostatic interactions at this position, although in the current study these ring atoms are slightly too far away from the Gln 273 side chain to form hydrogen bonds. Noticeably, there is a clear overlap between methyl and N1 probe favorable zones in the FAAH active site, possibly suggesting that the major interaction between the N1 probe and the ligands could be of a steric nature. This is further emphasized by the fact that there are no hydrogen-bond donors near the side chain of Leu 278. As with the favorable N1 regions, the disfavored N1 regions are also in agreement with the methyl probe (Figure 7b). With respect to the CA channel, placing an *ortho*- or *para*-substituent on the *O*-phenyl ring decreases inhibition activity. Furthermore, in *N*-alkyl/aryl binding region, N1 shares a similar disfavored region with the methyl probe by outlining the shape of the ACB channel. In addition, there is a disfavored N1 region close to Met 191 and Cys 269, which resembles the shape of the FAAH active site. Moreover, this region corresponds to the *para*-methoxycarbonyl substituents of **106** and **107**. The additional *ortho*-substituents of these compounds alters their binding conformations and also enhances their FAAH activity compared to the parent compounds,[49] but the *para*-substituent seems to be unfavorable for inhibitory activity.

The hydrogen-bond donor properties of the ligands were assessed with a carbonyl oxygen probe (O). The favorable and unfavorable regions are presented in Figure 7c. As with the N1 probe, the O regions follow the shapes of the steric contours. No corresponding interacting FAAH residues were identified to complement the favorable O regions, thus decreasing the value of the model in terms of hydrogen-bond donating features of the ligands. This is presumably due to the small number of ligands with hydrogen-bond donating moieties (excluding the invariable carbamate functionality) in the training set (Table 1 and Table 2).

When comparing the contours of the final CoMSIA (Figure 5) and GRID/GOLPE (Figure 7) models, both the CoMSIA hydrophobic descriptor and GRID methyl probe emphasize the importance of having the *O*-phenyl ring substituted at the *meta*-position. Both steric and hydrophobic CoMSIA descriptors penalize the ligands protruding towards the hydrophilic end of

the CA cavity, whereas no GOLPE contours can be observed in this region (at the applied coefficient levels). Interestingly, the disfavored CoMSIA electrostatic region partially overlaps with the disfavored GOLPE N1 region, giving further confidence of the detrimental effects of polar substituents at the *para*-position of the *O*-phenyl ring.

Conclusions

We have described the synthesis of a series 3-heterocyclephenyl *N*-alkylcarbamates as novel and potent FAAH inhibitors. The most potent compound, 3-(oxazol-2yl)phenyl cyclohexylcarbamate (**2a**), inhibited FAAH with a sub-nanomolar level IC_{50} value (IC_{50} = 0.74 nM). Moreover, the *N*-cyclohexyl carbamates with 1,2,3-thiadiazol-4-yl (**1b**) and tetrazolyl (**9a**) moieties were almost equally potent (IC_{50} = 1.0–1.1 nM). Furthermore, we have presented externally validated 3D-QSAR models for carbamates as FAAH inhibitors. Prior to QSAR analysis, we estimated the reactivity of our compounds. The 3D-QSAR models highlight the molecular features favorable, such as having the *O*-phenyl ring substituted at the *meta*-position, and detrimental, like having a rigid N-substituent, to FAAH inhibition. Consequently, these models make in silico design and evaluation of further carbamate optimizations possible, and also allows the prioritization of synthetic work. Finally, the applied automated docking scheme enables rapid protein-based alignment of large sets of carbamates.

Experimental Section

Chemistry

Commercially available starting materials were used without further purification. Solvents were distilled or dried over molecular sieves prior to use. All dry reactions were performed under argon in flame- or oven-dried glassware. Microwave assisted reactions were carried out using a CEM Discover™ microwave reactor. Analytical thin-layer chromatography (TLC) was carried out on Merck silica gel F_{254} (60 Å, 40–63 μm, 230–400 mesh) precoated aluminum sheets and detected under UV-light. Purification of reaction products was carried out by flash chromatography (FC) on J. T. Bakers silica gel for chromatography (pore size 60 Å, particle size 50 nm). The ^{1}H NMR and ^{13}C NMR spectra were recorded on a Bruker Avance 500 or 400 spectrometers operating at 500.1/400 MHz for ^{1}H and 125.1/100 MHz for ^{13}C. Chemical shifts are reported in ppm on the δ scale from an internal standard of solvent ($CDCl_3$ 7.26 and 77.0 ppm; [D_6]DMSO 2.50 and 39.52 ppm; CD_3OD 3.31 and 49.00 ppm). Elemental analyses (CHN) were recorded using a Thermo Quest CE Instrument EA 1110 CHNSO or Perkin–Elmer 2400 CHN elemental analyzers. Melting points were determined in open capillaries using a BÜCHI Melting Point B-545 or Stuart SMP and are uncorrected.

Ethyl 2-(1-(3-hydroxyphenyl)ethylidene)hydrazinecarboxylate (**14**) and 3-(1,2,3-Thiadiazol-4-yl)phenol (**15**) were prepared as described previously.[49] Compounds **1b–3, 5, 6a–8, 9c, 9e–f, 10, 11a–c, 11e, 12, 17a–b, 18a–b, 27, 33–38** were synthesised via known routes.[87–90] Full protocol and characterisation data for these compounds can be found in the Supporting Information.

2-(3-Methoxyphenyl)-4-phenyloxazole (17c): 3-Methoxybenzamide (1.5 g, 10 mmol, 1 equiv) and 2-bromo-1-phenylethanone (2.4 g, 12 mmol, 1.2 equiv) were added to round bottomed flask and irradiated (MW) for 5 min (power 200 W for 30 s, then 50 W, air cooling, T_{max} = 125 °C). The reaction mixture was dissolved in EtOAc (150 mL), CH_3OH (10 mL) and H_2O (50 mL). The organic phase was washed with saturated $NaHCO_3$, H_2O and brine, dried (Na_2SO_4), filtered and concentrated. Purification by flash chromatography (EtOAc/hexane, 5:95) gave **17c** (2.0 g, 79%) as a red oil (90% pure by ^{1}H NMR): ^{1}H NMR ($CDCl_3$, 400 MHz): δ = 7.96 (s, 1H), 7.84–7.81 (m, 2H), 7.72–7.70 (ddd, 1H), 7.66 (dd, J = 2.6, 1.6 Hz, 1H), 7.46–7.41 (m, 2H), 7.39 (t, J = 8.0 Hz, 1H), 7.36–7.30 (m, 1H), 7.01 (ddd, J = 8.3, 2.6, 1.0 Hz, 1H), 3.90 ppm (s, 3H); HRMS (ESI): m/z [M+Na]$^+$ calcd for $C_{16}H_{13}NO_2$: 274.0844, found: 274.0839.

3-(4-Phenyloxazol-2-yl)phenol (18c): Compound **17c** (150 mg, 0.6 mmol, 1 equiv) and *N*-butylpyridinium bromide (320 mg, 1.5 mmol, 2.5 equiv) were irradiated (MW) in a sealed tube for 3× 30 s (power 125 W, T_{max} = 100 °C). The reaction mixture was dissolved in EtOAc (50 mL) and the organic phase was washed with H_2O and brine, dried (Na_2SO_4), filtered and concentrated. Purification by flash chromatography (CH_2Cl_2, 100%) gave **18c** (84 mg, 60%) as a yellow wax: ^{1}H NMR (CD_3OD, 400 MHz): δ = 8.29 (s, 1H), 7.85–7.81 (m, 2H), 7.57 (ddd, J = 7.7, 1.5, 1.0 Hz, 1H), 7.51 (dd, J = 2.3, 1.7 Hz, 1H), 7.45–7.40 (m, 2H), 7.36–7.31 (m, 2H), 6.9 (ddd, J = 8.2, 2.5, 1.0 Hz, 1H), 4.17–4.03 (m, 1H), 2.10–1.99 (m, 2H), 1.79–1.59 (m, 4H), 1.57–1.46 ppm (m, 2H); ^{13}C NMR (CD_3OD, 100 MHz): δ = 163.6, 159.2, 143.2, 135.6, 132.4, 131.2, 129.8, 129.6, 129.2, 126.7, 118.9, 118.7, 114.1 ppm; HRMS (ESI): m/z [M−H]$^-$ calcd for $C_{15}H_{10}NO_2$: 236.0712, found: 236.0717.

3-(4-Phenyloxazol-2-yl)phenyl cyclopentylcarbamate (4): Crystallization (EtOAc/hexane) gave **4** (60 mg, 66%) as a white crystalline solid: mp 159–161 °C; ^{1}H NMR ($CDCl_3$, 400 MHz): δ = 7.97–7.93 (m, 2H), 7.91–7.88 (m, 1H), 7.84γ7.79 (m, 2H), 7.49–7.40 (m, 3H), 7.36–7.30 (m, 1H), 7.27–7.23 (m, 1H), 5.03 (br d, J = 6.8 Hz, 1H), 4.17–4.03 (m, 1H), 2.10–1.99 (m, 2H), 1.79–1.59 (m, 4H), 1.57–1.46 ppm (m, 2H); ^{13}C NMR ($CDCl_3$, 100 MHz): δ = 161.6, 154.1, 151.8, 142.5, 134,0 131.4, 130.1, 129.2, 129.1, 128.6, 126.1, 124.2, 123.7, 120.2, 53.5, 33.6, 24.0 ppm; Anal. calcd for $C_{21}H_{20}N_2O_3$: C 72.40, H 5.79, N 8.04, found: C 72.05, H 5.55, N 7.99.

5-(3-Hydroxyphenyl)-1*H*-tetrazole (30):[91] 3-Hydroxybenzonitrile (**29**, 1.43 g, 12 mmol, 1 equiv), Et_3NHCl (3.3 g, 24 mmol, 2 equiv) and NaN_3 (1.6 g, 8 mmol, 2 equiv) were refluxed in dry toluene (120 mL) for 20 h. The mixture was cooled to RT, diluted with H_2O (90 mL) and EtOAc (20 mL), and extracted with H_2O (20 mL). The aqueous phase was acidified by a dropwise addition of 32% HCl until a white solid precipitated. The precipitate was filtrated, washed with H_2O and dried to give **30** (2.2 g, 90%) as a white solid: mp 220–222 °C; ^{1}H NMR ([D_6]DMSO, 400 MHz): δ = 9.94 (s, 1H), 7.47–7.38 (m, 2H), 7.40 (t, J = 8 Hz, 1H), 6.98 ppm (ddd, J = 8, 2, 1 Hz, 1H); ^{13}C NMR ([D_6]DMSO, 100 MHz): δ = 158.0, 155.3 (br), 130.6, 125.1, 118.3, 117.6, 113.6 ppm.

3-(1*H*-Tetrazol-5-yl)phenyl cyclohexylcarbamate (31): This compound was isolated as described for **7a** and crystallized (H_2O/CH_3OH) giving **31** (1.1 g, 62%) as a white crystalline solid: mp 180–182 °C; ^{1}H NMR ([D_6]DMSO, 400 MHz): δ = 7.89 (t, J = 8.0 Hz, 1H), 7.78 (s, 1H), 7.62 (t, J = 7.9 Hz, 1H), 7.35 (d, J = 7.8 Hz, 1H), 3.42–3.29 (m, 1H), 1.91–1.81 (m, 2H), 1.77–1.66 (m, 2H), 1.62–1.53 (m, 1H), 1.36–1.20 (m, 4H), 1.19–1.06 ppm (m, 1H); ^{13}C NMR ([D_6]DMSO, 100 MHz): δ = 155.0, 153.1, 151.7, 130.6, 125.3, 124.6, 123.4, 120.2, 49.9, 32.5, 25.1, 24.6 ppm; HRMS (ESI): m/z [M+Na]$^+$ calcd for $C_{14}H_{17}N_5O_2Na$: 310.1280, found: 310.1291.

3-(2-Methyl-2*H*-tetrazol-5-yl)phenyl cyclohexylcarbamate (9a): This compound was prepared and worked up as described for **7b**. The isomers were separated by flash chromatography (CH_3OH/CH_2Cl_2, 0.5→1%) and major product was crystallized (EtOAc/hexane) giving **9a** (270 mg, 35%) as a white solid: mp 158–160 °C; ^{1}H NMR ($CDCl_3$, 400 MHz): δ = 7.97(d, J=7.8 Hz, 1H), 7.93–7.90 (m, 1H), 7.47 (t, J = 7.9 Hz, 1H), 7.28–7.23 (m, 1H), 7.97 (br d, J = 7.8 Hz, 1H), 4.39 (s, 3H), 3.65–3.52 (m, 1H), 2.07–1.98 (m, 2H), 1.80–1.70 (m, 2H), 1.68–1.59 (m, 1H), 1.45–1.33 (m, 2H), 1.30–1.17 ppm (m, 3H); ^{13}C NMR ($CDCl_3$, 100 MHz): δ = 164.7, 153.3, 151.5, 129.8, 128.5, 123.6, 123.5, 120.1, 50.2, 39.5, 33.2, 25.4, 24.7 ppm; Anal. calcd for $C_{15}H_{19}N_5O_2$: C 59.79, H 6.36, N 23.24, found: C 59.49, H 6.20, N 23.13.

3-(1-Methyl-1*H*-tetrazol-5-yl)phenyl cyclohexylcarbamate (9b): The minor product from preparation of **9a** was crystallized (EtOAc/hexane) giving **9b** (26 mg, 3%) as a white crystalline solid: mp 157–161 °C; ^{1}H NMR ($CDCl_3$, 400 MHz): δ = 7.61–7.51 (m, 3H), 7.40–7.32 (m, 1H), 5.08–4.97 (br d, 1H), 4.19 (s, 3H), 3.64–3.51 (m, 1H), 2.10–1.97 (m, 2H), 1.82–1.70 (m, 2H), 1.69–1.57 (m, 1H), 1.46–1.33 (m, 2H), 1.32–1.14 ppm (m, 3H); ^{13}C NMR ($CDCl_3$, 100 MHz): δ = 153.8, 153.0, 151.5, 130.3, 125.2, 124.6, 124.4, 122.1, 50.3, 35.1, 33.2, 25.4, 24.7 ppm; Anal. calcd for $C_{15}H_{19}N_5O_2$: C 59.79, H 6.36, N 23.24, found: C 59.80, H 6.30, N 23.07.

3-(Cyclohexylcarbamoyloxy)benzoic acid (9d): Crystallization (EtOAc/hexane) gave **9d** (280 mg, 73%) as a white solid: mp 205–206 °C; ^{1}H NMR ([D$_6$]DMSO, 400 MHz): δ = 13.13 (s, 1H), 7.83°7.75 (m, 2H), 7.61–7.58 (m, 1H), 7.50 (t, J = 7.9 Hz, 1H), 7.38–7.34 (m, 1H), 3.40–3.27 (m, 1H), 1.89–1.79 (m, 2H), 1.76–1.66 (m, 2H), 1.61–1.52 (m, 1H), 1.34–1.05 ppm (m, 5H); ^{13}C NMR ([D$_6$]DMSO, 100 MHz): δ = 166.6, 153.2, 151.1, 132.0, 129.6, 126.2, 125.7, 122.3, 49.8, 32.5, 25.1, 24.5 ppm; Anal. calcd for $C_{14}H_{17}NO_4$: C 63.87, H 6.51, N 5.32, found: C 63.95, H 6.60, N 5.61.

3-Hydroxybenzamide (40):[92] A solution of 3-cyanophenol (**29**) (295 mg, 2.48 mmol, 1 equiv) and $NaBO_3{\cdot}4H_2O$ (1.15 g, 7.45 mmol, 3 equiv) in H_2O (8 mL) was heated to 50 °C and CH_3OH (14 mL) was added until the mixture became clear. Stirring was continued at 50 °C for 70 h. Excess CH_3OH was evaporated and the remaining mixture was adjusted to pH 5 with concd HCl (aq). The mixture was extracted with CH_2Cl_2 and EtOAc (5×15 mL). The combined organic phases were washed with brine and dried (Na_2SO_4). Evaporation of solvent gave **40** (183 mg, 54%) as a white solid: mp 165–168 °C; ^{1}H NMR ([D$_6$]DMSO, 400 MHz): δ = 9.58 (s, 1H), 7.84 (br s, 1H), 7.29–7.20 (m, 4H), 6.89 ppm (ddd, J = 7.9, 2.5, 1.0 Hz, 1H).

3-Formylphenyl cyclohexylcarbamate (9g): Recrystallization from EtOAc/hexane gave **9g** (2.9 g, 69%) as a white crystalline solid; mp 120–122 °C; ^{1}H NMR ($CDCl_3$, 400 MHz); 9.92 (s, 1H), 7.71 (d, J = 7.6 Hz, 1H), 7.67–7.65 (m, 1H), 7.52 (t, J = 7.8 Hz, 1H), 7.43–7.39 (m, 1H), 5.01 (br d, J = 6.8 Hz, 1H), 3.63–3.51 (m, 1H), 2.09–1.98 (m, 2H), 1.81–1.71 (m, 2H), 1.68–1.59 (m, 1H), 1.45–1.32 (m, 2H), 1.30–1.14 ppm (m, 3H); ^{13}C NMR ($CDCl_3$, 100 MHz): δ = 191.4, 153.1, 151.7, 137.6, 129.9, 127.8, 126.4, 122.4, 50.3, 33.2, 25.4, 24.7 ppm; Anal. calcd for $C_{14}H_{17}NO_3$: C 68.00, H 6.93, N 5.66, found: C 67.83, H 6.86, N 5.65.

3-(4,5-Dihydro-1*H*-imidazol-2-yl)phenyl cyclohexylcarbamate (9h): A solution of **9g** (300 mg, 1.2 mmol, 1 equiv) in CH_2Cl_2 (10 mL) was treated with ethane-1,2-diamine (85 μL, 1.3 mmol, 1.05 equiv) at −2 °C (T_{bath}). The mixture was stirred for 30 min and *N*-bromosuccinimide (230 mg, 1.3 mmol, 1.05 equiv) was added. The mixture was allowed to warm to RT over 1 h and evaporated to dryness. The resulting solid was dissolved in 10% Et_3N in EtOAc and filtered through a pad of silica. The solution was concentrated and the residue was crystallized (EtOAc/CH_2Cl_2) to give **9h** (290 mg, 83%) as a white crystalline solid: mp 139–141 °C; ^{1}H NMR ($CDCl_3$, 400 MHz): δ = 7.60 (dt, J = 7.7, 1.3 Hz, 1H), 7.53 (s, 1H) 7.37 (t, J = 7.9 Hz, 1H), 7.20 (dd, J = 8.2, 1.5 Hz, 1H), 5.07 (br d, J = 7.5 Hz, 1H), 3.77 (br s, 4H), 3.60–3.48 (m, 1H), 2.05–1.96 (m, 2H), 1.79–1.69 (m, 2H), 1.67–1.58 (m, 1H), 1.43–1.31 (m, 2H), 1.28–1.13 ppm (m, 3H); ^{13}C NMR (CD_3OD, 100 MHz): δ = 166.7, 156.0, 152.8, 132.5, 130.4, 125.4, 125.0, 121.8, 51.7, 50.4, 34.0, 26.6, 26.1 ppm; Anal. calcd for $C_{16}H_{21}N_3O_2$: C 66.88, H 7.37, N 14.62, found: C 66.54, H 7.33, N 14.27.

3-(2-Methoxyethoxymethoxy)-benzonitrile (32):[87,93] An ice-cold solution of 3-cyanophenol (**29**, 1.79 g, 15 mmol, 1 equiv) and Et_3N (2.7 mL, 19.5 mmol, 1.3 equiv) in dry THF (60 mL) was treated dropwise with methoxyethoxymethyl chloride (2.7 mL, 24.0 mmol, 1.6 equiv) under Ar. The mixture was allowed to warm to RT and then heated at reflux overnight. The mixture was poured into EtOAc, washed with H_2O and brine, and dried (Na_2SO_4). Evaporation of solvent gave **32** (2.74 g, 88%) as a white solid: ^{1}H NMR ($CDCl_3$, 500 MHz): δ = 7.39–7.34 (m, 2H), 7.30–7.27 (m, 2H), 5.28 (s, 2H), 3.83–3.81 (m, 2H), 3.56–3.54 (m, 2H), 3.37 ppm (s, 3H); ^{13}C NMR ($CDCl_3$, 125.1 MHz): δ = 157.4, 130.3, 126.6, 121.2, 119.7, 118.6, 113.3, 93.5, 71.5, 68.0, 59.0 ppm.

3-(5-Butyl-1,2,4-oxadiazol-3-yl)phenyl cyclohexylcarbamate (11d): Purification by flash chromatography (EtOAc/PE) and crystallization (EtOAc/hexane) gave **11d** (167 mg, 49%) as a white crystalline solid: mp 96.8–97.7 °C; ^{1}H NMR ($CDCl_3$, 500.1 MHz): δ = 7.75 (d, J = 7.7 Hz, 1H), 7.85–7.84 (m, 1H), 7.45 (t, J = 7.9 Hz, 1H), 7.28 (d, J = 8.2 Hz, 1H), 4.93 (d, J = 6.9 Hz, 1H), 3.60–3.55 (m, 1H), 2.94 (t, J = 7.6 Hz, 1H), 2.02 (br d, J = 9.7 Hz, 2H), 1.88–1.82 (m, 2H), 1.76–1.74 (m, 2H), 1.65–1.62 (m, 1H), 1.49–1.34 (m, 5H), 1.27–1.16 (m, 3H), 0.97 ppm (t, J = 7.4 Hz, 3H); ^{13}C NMR ($CDCl_3$, 125.1 MHz): δ = 180.1, 167.7, 153.3, 151.4, 129.7, 128.2, 124.4, 124.0, 120.8, 50.2, 33.2, 28.6, 26.3, 25.4, 24.7, 22.1, 13.5 ppm; Anal. calcd for $C_{19}H_{25}N_3O_3$: C 66.45, H 7.34, N 12.24, found: C 66.39, H 7.41, N 12.39.

Dimethyl 4-hydroxyphtalate (42):[94] 3-Hydroxyphtalic acid (**41**, 360 mg, 2.0 mmol, 1 equiv) was dissolved in CH_3OH (20 mL), and concd H_2SO_4 (11 μL, 0.2 mmol, 0.1 equiv) was added to the mixture. The mixture was refluxed for 24 h, cooled to RT, poured into saturated $NaHCO_3$ (30 mL), and most of the CH_3OH was evaporated. The mixture was extracted with EtOAc and the combined organic phases were dried (Na_2SO_4), filtered and evaporated giving **42** (400 mg, 95%) as a white solid: mp 110–111 °C; ^{1}H NMR ($CDCl_3$, 500.1 MHz): δ = 7.74 (d, 1H, J = 8.6 Hz), 7.24 (br s, 1H), 7.01 (d, 1H, J = 2.6 Hz), 6.92 (dd, 1H, J = 8.4, 2.6 Hz) 3.90 (s, 3H) 3.86 ppm (s, 3H); ^{13}C NMR ($CDCl_3$, 125.1 MHz): δ = 169.6, 167.2, 159.4, 135.6, 131.9, 121.5, 117.3, 115.3, 53.0, 52.5 ppm.

In vitro assays

Animals and preparation of rat brain homogenate for FAAH assay: Eight-week old male Wistar rats were used in these studies. All animal experiments were approved by the local ethics committee. The animals were housed with a standard 12 h lights on/off cycle (lights on at 07:00) with water and food available ad libitum.

The rats were decapitated, whole brains minus cerebellum were dissected and homogenized in one volume (*v*/*w*) of ice-cold 0.1 M potassium phosphate buffer (pH 7.4) with a Potter–Elvehjem homogenizer (Heidolph, Schwabach, Germany). The homogenate was centrifuged at 10000 *g* for 20 min at 4 °C and the resulting supernatant was used as a source of FAAH. The protein concentration of

the supernatant (7.2 mg mL^{-1}) was determined by the method of Bradford with bovine serum albumin (BSA) as a standard.[95] Aliquots of the supernatant were stored at −80 °C until use.

Animals and preparation of rat cerebellar membranes for MGL assay: Four-week old male Wistar rats were used in these studies. All animal experiments were approved by the local ethics committee. The animals were housed with a standard 12 h lights on/off cycle (lights on at 07:00), with water and food available ad libitum. The rats were decapitated 8 h after lights on (1500 h) and the whole brains were removed, dipped in isopentane on dry ice and stored at −80 °C. Membranes were prepared as previously described.[96] Briefly, cerebella (minus brain stem) from eight animals were weighed and homogenized in nine volumes of ice-cold sucrose (0.32 M) with a glass Teflon homogenizer. The crude homogenate was centrifuged at low speed (1000 *g* for 10 min at 4 °C) and the pellet was discharged. The supernatant was centrifuged at high speed (100 000 *g* for 10 min at 4 °C). The pellet was resuspended in ice-cold deionized water and washed twice, repeating the high-speed centrifugation. Finally, membranes were resuspended in 50 mM Tris-HCl, pH 7.4 with 1 mM EDTA and aliquoted for storage at −80 °C. The protein concentration of the final preparation, measured by the Bradford method,[95] was 11 mg mL^{-1}.

In vitro assay for FAAH activity: The assay for FAAH has been described previously.[51] The endpoint enzymatic assay was developed to quantify FAAH activity with tritium-labeled anandamide (AEA; [^{3}H]ethanolamine). The assay buffer was 50 mM Tris-HCl (pH 7.4); 1 mM EDTA and test compounds were dissolved in DMSO (the final DMSO concentration was not more than 5% *v/v*). The incubations were performed in the presence of 0.5% (*w/v*) BSA (essentially fatty acid free). Test compounds were preincubated with rat brain homogenate protein (18 μg) for 10 min at 37 °C and incubations started by adding AEA (2 μM, containing 50×10^{-3} μM of 40–60 Ci mmol^{-1} [^{3}H]AEA). The hydrolysis of [^{3}H]AEA to [^{3}H]ethanolamine was measured for radioactivity by liquid scintillation counting (Wallac 1450 MicroBeta; Wallac Oy, Finland).

In vitro assay for MGL activity: The assay for MGL has been described previously.[31] The endpoint enzymatic assay was developed to quantify MGL activity against 2-arachidonoylglycerol (2-AG) hydrolysis. The assay buffer was 50 mM Tris-HCl, pH 7.4; 1 mM EDTA and test compounds were dissolved in DMSO (the final DMSO concentration was not more than 5% *v/v*). The incubations were performed in the presence of 0.5% (*w/v*) BSA (essentially fatty acid free). hrMGL was preincubated with test compounds for 10 min at 37 °C, and incubations started by an addition of 2-AG (50 μM). The formation of arachidonic acid and depletion of 2-AG (and 1-AG) was measured by HPLC, as previously described.[29]

Data analyses: The results from the enzyme inhibition experiments are presented as the mean ±95% confidence intervals of at least three independent experiments performed in duplicate. Data analyses for the concentration–response curves were calculated as nonlinear regressions using GraphPad Prism 4.0 for Windows.

Computational protocol

Structure construction: All compound structures were constructed using SYBYL 8.0[97] and optimized employing the Merck molecular force field (MMFF94s)[98] with BFGS minimizer to an energy gradient of 0.001 kcal(mol*Å)$^{-1}$. Atom types, automatically assigned by SYBYL, were inspected and fixed with an in-house script. The X-ray crystal structure of murine FAAH complexed with methyl arachidonyl fluorophosphonate (MAFP) (PDB: 1MT5)[36] was used as the protein structure for docking calculations. Monomeric enzyme (chain A) was extracted from the crystal data, the missing side chain atoms (none at the active site) were added with the SYBYL Biopolymer module using suitable conformations with minimal structural violations from the Lovell rotamer library.[99] The side chain amide groups of Gln 48, Gln 60, Gln 124, Asn 159, Gln 189, Gln 519 and Gln 570 were flipped to maximize internal hydrogen bonding, the MAFP atoms were removed, hydrogen atoms were added, and side chain atoms were optimized in Amber FF99[100] as implemented in SYBYL (steepest descent, 300 iterations). The orientation of the hydrogen atoms of amino acids in the catalytic region were inspected to ensure that a hydrogen bond was formed between the hydroxy groups of Ser 217 and Ser 241 and between the side chains of Ser 217 and Lys 142. All the computations and visualization of the results were done using a Linux PC cluster and a Mac Pro workstation. VMD versions 1.8.6 and 1.8.7beta were used to render the figures.[101]

Ligand alignment by molecular docking: In order to use protein-based ligand alignment for the 3D-QSAR modeling, molecular docking with Surflex-Dock™ 2.1[70] was used. Surflex-Dock™ uses protomol—a representation of the active site with steric and hydrogen bonding probes—to direct the initial placements of the ligands during the posing phase of the docking process. In the current study, protomol was generated using a ligand-based mode of construction with default settings. Compound **87** was placed into the FAAH active site so that the carbonyl oxygen was interacting with the backbone atoms of the FAAH oxyanion hole, the *N*-hexyl moiety was pointing towards the acyl chain binding (ACB) channel, and the *O*-phenyl ring was pointing towards the cytoplasmic access (CA) channel.

In our initial experiments, we tested several sets of protomols and docking settings. However, there was a lot of variation in the placement of the structurally similar ligands, and even with manually selecting the poses, we were unable to build predictive QSAR models (data not shown). In order to create a fast, consistent and automated docking scheme for 3D-QSAR purposes, we resorted to a new feature introduced in Surflex-Dock™ 2.1: fragment-guided docking.[70] We used a NC(=O) fragment taken from the top-ranked docked conformation (with no fragment guiding) of the potent carbamate **1a** (see Supporting Information, figure S1).[49] Furthermore, to emphasize the importance of interactions between the oxyanion hole, the catalytic residues and the carbamate functionality in the putative initial binding conformation, we applied a penalty value for conformations deviating from the predefined fragment ("-cpen" option in Surflex-Dock™ 2.1). Values up to the maximum value of 100 pK_d Å^{-2} were tested when determining the alignment to be used for the subsequent 3D-QSAR models.

For the actual docking processes, we used settings aimed at thorough sampling. Prior to docking, Surflex-Dock™ was allowed to pre-minimize the ligands with the implemented BFGS method employing DREIDING force field.[102] To enhance the sampling during the ligand posing in docking, the number of additional conformations per molecule, and the maximum number of conformations per fragment were set to 140 and 200, respectively. Surflex-Dock™ was allowed to treat ring systems flexibly. Additionally, ligands were relaxed in the active site after the docking using the DREIDING force field method. The 20 best-ranked conformations for each ligand were retained, but after visual inspection the best-ranked conformation was selected if not mentioned otherwise.

Atomic point charges: The ESP-fitted (Merz–Singh–Kollman scheme) ab initio charges were calculated with Gaussian 03 using Hartree–

Fock level of theory and 6–311G** basis set.[103,104] The semiempirical ESP-fitted MNDO charges were calculated with MOPAC 6.0.[105] The Gasteiger–Hückel topological charges were computed as implemented in SYBYL.

Molecular orbitals and reactivity: Starting from the docked conformations (the best-ranking conformations at penalty value of 1 pK_d Å^{-2}, post-docking minimization enabled), the compounds were optimized in Hartree–Fock/6–311G** level of theory with Gaussian 03.[104] HOMO (E_{HOMO}) and LUMO (E_{LUMO}) energies were derived from these quantum chemical calculations. Additionally, the chemical hardness of the compound was evaluated. Originally, the chemical hardness (η) was formulated from the Pearson acid–base concept,[106,107] and is defined as:

$$\eta = \frac{1}{2}\left(\frac{\partial^2 E}{\partial N^2}\right)_v \quad (1)$$

where E is the total energy of the system and N is the number of electrons in the system. By using Koopmans' theorem in the Hartree–Fock scheme,[108] we calculated an approximation of the chemical hardness[65] by:

$$\eta = \frac{1}{2}(E_{LUMO} - E_{HOMO}) \quad (2)$$

The degree of correlation between the orbital energies, chemical hardness, and FAAH pIC_{50} inhibition values was determined by linear regression (calculated with SPSS 16.0 for Mac).

Data sets: A total of 99 carbamate derivatives (33 reported here, 66 previously described[41,49,50]), with in-house measured FAAH IC_{50} inhibition data, were used to derive the 3D-QSAR models (Table 1 and Table 2). To gain further confidence in the resulting models, we chose to divide the compounds into a training set for the actual model building, and into a test set for external prediction validation. Training and test sets should be balanced between representativeness and diversity with similar response distributions (inhibition data).[63] In this study, we applied *k*-dissimilarity (OptiSim) selection to derive the sets.[109,110] OptiSim uses Tanimoto coefficients, based on UNITY two-dimensional fingerprints, to measure the dissimilarity of the compounds. Here, we used a subsample size (*k*) value of 4 to select 25 compounds for the test set, leaving 74 compounds for the model building. The representativeness and diversity of the data sets were visualized in MOE default two-dimensional molecular descriptor chemical space with principal component analysis (with descriptor values autoscaled to unit variance).[111]

CoMSIA: Initially, the CoMSIA method[52,112,113] was used to generate 3D-QSAR models for the different ligand alignments resulting from the Surflex-Dock™ docking runs with variable penalty values (see above), and to select the optimal penalty value and the alignment for further models. The SYBYL default settings were applied for calculation of the CoMSIA steric, electrostatic, hydrophobic, hydrogen-bond acceptor, and hydrogen-bond donor similarity indices. A column filtering value of 0.001 kcal mol^{-1} was applied in the cross-validation calculations unless mentioned otherwise. Measured enzyme inhibition concentrations (transformed to $-\log[IC_{50}]$) were used as dependent variables. Leave-one-out (LOO) and leave-half-out (LHO) cross-validation schemes were used to determine the number of components for the PLS models. For LHO, the procedure was repeated 20 times and the average statistical values were calculated.

Additionally, in order to enhance the models and their CoMSIA fields, and also to tighten the grid spacing, a technique called region focusing[75] was applied. Apart from using StDev*Coefficient as the weighing value, default SYBYL settings were applied. Weight exponential factor was set to 0.3, 0.5 and 0.8. The default value of CoMSIA grid spacing is 2.0 Å, so we used finer grid spacing values of 1.0 and 0.5 Å in the focusing.

To estimate the stability of the models with respect to random noise in the data (i.e., sensitivity to chance correlations), the models were subjected to the progressive scrambling procedure available in SYBYL.[76] Twenty independent scrambling runs using the SAMPLS[69] algorithm, with 100 scramblings in each, were calculated and the statistical parameters were determined at the critical threshold level of perturbation ($s = 0.85$). The progressive scrambling results were used to aid the determination of the number of components in the final CoMSIA models, and furthermore to select only the stable models for test set validation. The default contour levels were used when visualizing the CoMSIA (StDev*Coefficient) fields.

GRID/GOLPE: With the aim of gaining access to a more diverse set of QSAR variables, and also more powerful variable selection tools, GRID/GOLPE 3D-QSAR method was also applied. The test and training sets, and the compound alignments were those used to derive the CoMSIA models. GRID[84,114] software was used to calculate the interaction energies between the aligned compounds and the selected probes. The carbon (C3) probe was chosen to resemble the hydrophobic and steric contacts, whereas the sp^2 carbonyl oxygen (O) and neutral flat amide nitrogen (N1) probes were chosen to account for the hydrogen-bond donor and acceptor capabilities of the compounds, respectively. GRID was allowed to determine the grid dimensions automatically with a grid spacing of 0.5 Å. The default partial charge calculation method was used.

The interaction energies at each lattice point were subsequently used as independent variables with pIC_{50} values as dependent variables to create the 3D-QSAR PLS models with GOLPE[85] (version 4.6). It is well known that the initial number of X-variables must be processed to decrease the noise and interaction points unimportant for the activity prediction. Firstly, the advanced pretreatment module of GOLPE was used to replace (highly repulsive) positive variable values with the cutoff value of $+4.0$ kcal mol^{-1}. This removes the artificial variance arising from the grid points close to the van der Waals surface of the compounds. Negative values larger than -0.01 kcal mol^{-1} and positive values smaller than $+0.1$ kcal mol^{-1} were zeroed to diminish the amount noise in the data. Variables with low standard deviation and thus with small variance were set inactive with a cutoff value of 0.1. Finally, all two-level and three-level variables were removed. These are variables with only a few values within the data set, and using them might lead to misleading results.

Following the pretreatment, PLS models were created to ensure the model quality was high enough (in terms of internal predictivity) for the subsequent variable selection. Neighboring variables with similar chemical and statistical information were grouped with smart region definition (SRD) algorithm of GOLPE. Groups were generated using a maximum number of components of five, with critical distance of 2.0 Å along with setting the collapsing distance to the maximal value. Next, the groups were used in the fractional factorial design (FFD) scheme to evaluate the effect of each group in the predictivity of the model, and thus include only the most relevant variables into the resulting PLS models. A maximum of five components and five random groups of inhibitors in

25 validation runs were used in the FFD selection. The FFD procedure was repeated until the external predictivity of the resulting models was not improved.

Test set correlation validation: The resulting CoMSIA and GRID/GOLPE models were used to predict pIC_{50} of FAAH inhibition of the test set compounds. Predicted versus experimental pIC_{50} plots were used to determine: the correlation coefficient of the best-fit line (R^2), the correlation coefficient of the zero-intercept line (R_0^2), and the slope of the zero-intercept line (k). Also, the reverse relationship experimental versus predicted pIC_{50} plots were created of which the corresponding values, R'^2, $R'_0{}^2$ and k', were calculated. The models were then evaluated according to the criteria suggested by Golbraikh and Tropsha.[73]

Acknowledgements

We would like to thank Dr. Maija Lahtela-Kakkonen, Dr. Tuomo Laitinen, Mr. Tuomo Kalliokoski, Ms. Erja Kivioja and Ms. Minna Glad for technical help. CSC - Scientific Computing, Ltd. is acknowledged for computational resources. The National Graduate School in Informational and Structural Biology (ISB), the National Technology Agency of Finland, the Finnish Cultural Foundation, the Graduate School for Organic Chemistry and Chemical Biology (GSOCCB) and the Academy of Finland (grants 110277 and 128056) have provided financial support for this study.

Keywords: ab initio calculations · molecular modeling · FAAH inhibitors · phenyl *N*-alkylcarbamates · structure–activity relationships

[1] W. A. Devane, L. Hanus, A. Breuer, R. G. Pertwee, L. A. Stevenson, G. Griffin, D. Gibson, A. Mandelbaum, A. Etinger, R. Mechoulam, *Science* **1992**, *258*, 1946 – 1949.
[2] R. Mechoulam, S. Ben-Shabat, L. Hanus, M. Ligumsky, N. E. Kaminski, A. R. Schatz, A. Gobher, S. Almog, B. R. Martin, D. R. Compton, R. G. Pertwee, G. Griffin, M. Bayewitch, J. Barg, Z. Vogel, *Biochem. Pharmacol.* **1995**, *50*, 83 – 90.
[3] T. Sugiura, S. Kondo, A. Sukawaga, S. Nakane, A. Shinoda, K. Itoh, A. Yamasita, K. Waku, *Biochem. Biophys. Res. Commun.* **1995**, *215*, 89 – 97.
[4] W. A. Devane, F. A. Dysarz III, M. R. Johnson, L. S. Melvin, A. C. Howlett, *Mol. Pharmacol.* **1988**, *34*, 605 – 613.
[5] L. A. Matsuda, S. J. Lolait, M. J. Brownstein, A. C. Young, T. I. Bonner, *Nature* **1990**, *346*, 561 – 564.
[6] S. Munro, K. L. Thomas, M. Abu-Shaar, *Nature* **1993**, *365*, 61 – 65.
[7] V. Di Marzo, M. Bifulco, L. De Petrocellis, *Nat. Rev. Drug Discov.* **2004**, *3*, 771 – 784.
[8] a) D. M. Lambert, C. J. Fowler, *J. Med. Chem.* **2005**, *48*, 5059 – 5087; b) S. M. Saario, J. T. Laitinen, *Basic Clin. Pharmacol. Toxicol.* **2007**, *101*, 287 – 293; c) V. Di Marzo, *Nat. Rev. Drug Discovery* **2008**, *7*, 438 – 455.
[9] S. Kathuria, S. Gaetani, D. Fegley, F. Valiño, A. Duranti, A. Tontini, M. Mor, G. Tarzia, G. La Rana, A. Calignano, A. Giustino, M. Tattoli, M. Palmery, V. Cuomo, D. Piomelli, *Nat. Med.* **2003**, *9*, 76 – 81.
[10] V. Di Marzo, S. K. Goparaju, L. Wang, J. Liu, S. Bátkai, Z. Járai, F. Fezza, G. I. Miura, R. D. Palmiter, T. Sugiura, G. Kunos, *Nature* **2001**, *410*, 822 – 825.
[11] T. Järvinen, D. W. Pate, K. Laine, *Pharmacol. Ther.* **2002**, *95*, 203 – 220.
[12] L. Hanus, A. Breuer, S. Tchilibon, S. Shiloah, D. Goldenberg, M. Horowitz, R. G. Pertwee, R. A. Ross, R. Mechoulam, E. Fride, *Proc. Natl. Acad. Sci. USA* **1999**, *96*, 14228 – 14233.
[13] B. F. Cravatt, D. K. Giang, S. P. Mayfield, D. L. Boger, R. A. Lerner, N. B. Gilula, *Nature* **1996**, *384*, 83 – 87.
[14] B. Q. Wei, T. S. Mikkelsen, M. K. McKinney, E. S. Lander, B. F. Cravatt, *J. Biol. Chem.* **2006**, *281*, 36569 – 36578.
[15] T. P. Dinh, D. Carpenter, F. M. Leslie, T. F. Freund, I. Katona, S. L. Sensi, S. Kathuria, D. Piomelli, *Proc. Natl. Acad. Sci. USA* **2002**, *99*, 10819 – 10824.
[16] a) K. Ahn, M. K. McKinney, B. F. Cravatt, *Chem. Rev.* **2008**, *108*, 1687 – 1707; b) M. Seierstad, J. G. Breitenbucher, *J. Med. Chem.* **2008**, *51*, 7327 – 7343; c) S. Vandevoorde, *Curr. Top. Med. Chem.* **2008**, *8*, 247 – 267; d) A. Viso, J. A. Cisneros, S. Ortega-Gutiérrez, *Curr. Top. Med. Chem.* **2008**, *8*, 231 – 246.
[17] V. Di Marzo, T. Bisogno, L. De Petrocellis, D. Melck, P. Orlando, J. A. Wagner, G. Kunos, *Eur. J. Biochem.* **1999**, *264*, 258 – 267.
[18] V. Di Marzo, L. De Petrocellis, N. Sepe, A. Buono, *Biochem. J.* **1996**, *316*, 977 – 984.
[19] C. Hardouin, M. J. Kelso, F. A. Romero, T. J. Rayl, D. Leung, I. Hwang, B. F. Cravatt, D. L. Boger, *J. Med. Chem.* **2007**, *50*, 3359 – 3368.
[20] M. Mor, S. Rivara, A. Lodola, P. V. Plazzi, G. Tarzia, A. Duranti, A. Tontini, G. Piersanti, S. Kathuria, D. Piomelli, *J. Med. Chem.* **2004**, *47*, 4998 – 5008.
[21] K. Ahn, D. S. Johnson, L. R. Fitzgerald, M. Liimatta, A. Arendse, T. Stevenson, E. T. Lund, R. A. Nugent, T. K. Nomanbhoy, J. P. Alexander, B. F. Cravatt, *Biochemistry* **2007**, *46*, 13019 – 13030.
[22] G. G. Muccioli, N. Fazio, G. K. Scriba, W. Poppitz, F. Cannata, J. H. Poupaert, J. Wouters, D. M. Lambert, *J. Med. Chem.* **2006**, *49*, 417 – 425.
[23] X. Wang, K. Sarris, K. Kage, D. Zhang, S. P. Brown, T. Kolasa, C. Surowy, O. F. El Kouhen, S. W. Muchmore, J. D. Brioni, A. O. Stewart, *J. Med. Chem.* **2009**, *52*, 170 – 180.
[24] A. Minkkilä, S. M. Saario, H. Käsnänen, J. Leppänen, A. Poso, T. Nevalainen, *J. Med. Chem.* **2008**, *51*, 7057 – 7060.
[25] A. Minkkilä, J. R. Savinainen, H. Käsnänen, H. Xhaard, T. Nevalainen, J. T. Laitinen, A. Poso, J. Leppänen, S. M. Saario, *ChemMedChem* **2009**, *4*, 1253 – 1259.
[26] a) A. H. Lichtman, D. Leung, C. C. Shelton A. Saghatelian, C. Hardouin, D. L. Boger, B. F. Cravatt, *J. Pharmacol. Exp. Ther.* **2004**, *311*, 441 – 448; b) L. Chang, L. Luo, J. A. Palmer, S. Sutton, S. J. Wilson, A. J. Barbier, J. G. Breitenbucher, S. R. Chaplan, M. Webb, *Br. J. Pharmacol.* **2006**, *148*, 102 – 113; c) M. Scherma, J. Medalie, W. Fratta, S. K. Vadivel, A. Makriyannis, D. Piomelli, E. Mikics, J. Haller, S. Yasar, G. Tanda, S. R. Goldberg, *Neuropharmacology* **2008**, *54*, 129 – 140; d) K. Ahn, D. S. Johnson, M. Mileni, D. Beidler, J. Z. Long, M. K. McKinney, E. Weerapana, N. Sadagopan, M. Liimatta, S. E. Smith, S. Lazerwith, C. Stiff, S. Kamtekar, K. Bhattacharya, Y. Zhang, S. Swaney, K. Van Becelaere, R. C. Stevens, B. F. Cravatt, *Chem. Biol.* **2009**, *16*, 411 – 420.
[27] S. K. Goparaju, N. Ueda, H. Yamaguchi, S. Yamamoto, *FEBS Lett.* **1998**, *422*, 69 – 73.
[28] H. Tornqvist, P. Belfrage, *J. Biol. Chem.* **1976**, *251*, 813 – 819.
[29] S. M. Saario, J. R. Savinainen, J. T. Laitinen, T. Järvinen, R. Niemi, *Biochem. Pharmacol.* **2004**, *67*, 1381 – 1387.
[30] T. Sakurada, A. Noma, *J. Biochem.* **1981**, *90*, 1413 – 1419.
[31] S. M. Saario, O. M. H. Salo, T. Nevalainen, A. Poso, J. T. Laitinen, T. Järvinen, R. Niemi, *Chem. Biol.* **2005**, *12*, 649 – 659.
[32] N. Matuszak, G. G. Muccioli, G. Labar, D. M. Lambert, *J. Med. Chem.* **2009**; DOI: 10.1021/jm900461w.
[33] G. Labar, C. Bauvois, G. G. Muccioli, J. Wouters, D. M. Lambert, *ChemBioChem* **2007**, *8*, 1293 – 1297.
[34] A. R. King, A. Lodola, C. Carmi, J. Fu, M. Mor, D. Piomelli, *Br. J. Pharmacol.* **2009**, *157*, 974 – 983.
[35] a) J. Z. Long, W. Li, L. Booker, J. J. Burston, S. G. Kinsey, J. E. Schlosburg, F. J. Pavón, A. M. Serrano, D. E. Selley, L. H. Parsons, A. H. Lichtman, B. F. Cravatt, *Nat. Chem. Biol.* **2009**, *5*, 37 – 44; b) J. Z. Long, D. K. Nomura, B. F. Cravatt, *Chem. Biol.* **2009**, *16*, 744 – 753.
[36] M. H. Bracey, M. A. Hanson, K. R. Masuda, R. C. Stevens, B. F. Cravatt, *Science* **2002**, *298*, 1793 – 1796.
[37] a) M. Mileni, D. S. Johnson, Z. Wang, D. S. Everdeen, M. Liimatta, B. Pabst, K. Bhattacharya, R. A. Nugent, S. Kamtekar, B. F. Cravatt, K. Ahn, R. C. Stevens, *Proc. Natl. Acad. Sci. USA* **2008**, *105*, 12820 – 12824; b) M. Mileni, J. Garfunkle, J. K. DeMartino, B. F. Cravatt, D. L. Boger, R. C. Stevens, *J. Am. Chem. Soc.* **2009**, *131*, 10497 – 10506.
[38] G. Labar, F. Borel, C. Bauvois, J.-L.Ferrer, J. Wouters, D. M. Lambert, *19th Annual Symposium on Cannabinoids* **2009**, Burlington, Vermont (USA), International Cannabinoid Research Society, pp. 44.
[39] A. L. Bowman, A. Makriyannis, *J. Comput. Aided Mol. Des.* **2009**, *23*, 799 – 806.

[40] G. Tarzia, A. Duranti, G. Gatti, G. Piersanti, A. Tontini, S. Rivara, A. Lodola, P. V. Plazzi, M. Mor, S. Kathuria, D. Piomelli, *ChemMedChem* **2006**, *1*, 130 – 139.
[41] M. J. Myllymäki, H. Käsnänen, A. O. Kataja, M. Lahtela-Kakkonen, S. M. Saario, A. Poso, A. M. P. Koskinen, *Eur. J. Med. Chem.* **2009**, *44*, 4179 – 4191.
[42] A. Lodola, M. Mor, J. C. Hermann, G. Tarzia, D. Piomelli, A. J. Mulholland, *Chem. Commun.* **2005**, 4399 – 4401.
[43] I. Tubert-Brohman, O. Acevedo, W. L. Jorgensen, *J. Am. Chem. Soc.* **2006**, *128*, 16904 – 16913.
[44] A. Lodola, M. Mor, J. Zurek, G. Tarzia, D. Piomelli, J. N. Harvey, A. J. Mulholland, *Biophys. J.* **2007**, *92*, L20 - L22.
[45] C. R. Guimarães, D. L. Boger, W. L. Jorgensen, *J. Am. Chem. Soc.* **2005**, *127*, 17377 – 17384.
[46] A. Lodola, M. Mor, S. Rivara, C. Christov, G. Tarzia, D. Piomelli, A. J. Mulholland, *Chem. Commun.* **2008**, 214 – 216.
[47] G. Tarzia, A. Duranti, A. Tontini, G. Piersanti, M. Mor, S. Rivara, P. V. Plazzi, C. Park, S. Kathuria, D. Piomelli, *J. Med. Chem.* **2003**, *46*, 2352 – 2360.
[48] M. Mor, A. Lodola, S. Rivara, F. Vacondio, A. Duranti, A. Tontini, S. Sanchini, G. Piersanti, J. R. Clapper, A. R. King, G. Tarzia, D. Piomelli, *J. Med. Chem.* **2008**, *51*, 3487 – 3498.
[49] A. Minkkilä, M. J. Myllymäki, S. M. Saario, J. A. Castillo-Melendez, A. M. P. Koskinen, C. J. Fowler, J. Leppänen, T. Nevalainen, *Eur. J. Med. Chem.* **2009**, *44*, 2994 – 3008.
[50] M. J. Myllymäki, S. M. Saario, A. O. Kataja, J. A. Castillo-Melendez, T. Nevalainen, R. O. Juvonen, T. Järvinen, A. M. P. Koskinen, *J. Med. Chem.* **2007**, *50*, 4236 – 4242.
[51] S. M. Saario, A. Poso, R. O. Juvonen, T. Järvinen, O. M. H. Salo, *J. Med. Chem.* **2006**, *49*, 4650 – 4656.
[52] G. Klebe, U. Abraham, T. Mietzner, *J. Med. Chem.* **1994**, *37*, 4130 – 4146.
[53] C. D. Hurd, R. I. Mori, *J. Am. Chem. Soc.* **1955**, *77*, 5359 – 5364.
[54] M. A. Abramov, W. Dehaen, B. D'hooge, M. L. Petrov S. Smeets, S. Toppet, M. Voets, *Tetrahedron* **2000**, *56*, 3933 – 3940.
[55] a) H. Bredereck, G. Theilig, *Chem. Ber.* **1953**, *86*, 88 – 95; b) H. Bredereck, R. Gompper, *Chem. Ber.* **1954**, *87*, 700 – 707.
[56] S. M. S. Chauhan, N. J. Jain, *J. Chem. Res.* **2004**, 693 – 694.
[57] H. Fujioka, K. Murai, Y. Ohba, A. Hiramatsu, Y. Kita, *Tetrahedron Lett.* **2005**, *46*, 2197 – 2200.
[58] K. Koguro, T. Oga, S. Mitsui, R. Orita, *Synthesis* **1998**, 910 – 914.
[59] P. C. Unangst, G. P. Shrum, D. T. Connor, R. D. Dyer, D. J. Schrier, *J. Med. Chem.* **1992**, *35*, 3691 – 3698.
[60] A. R. Gangloff, J. Litvak, E. J. Shelton, D. Sperandio, V. R. Wang, K. D. Rice, *Tetrahedron Lett.* **2001**, *42*, 1441 – 1443.
[61] J. P. Alexander, B. F. Cravatt, *Chem. Biol.* **2005**, *12*, 1179 – 1187.
[62] E. Basso, A. Duranti, M. Mor, D. Piomelli, A. Tontini, G. Tarzia, P. Traldi, *J. Mass. Spectrom.* **2004**, *39*, 1450 – 1455.
[63] a) A. Fioni, F. Vacondio, M. Mor, C. Silva, A. Lodola, A. Duranti, A, Tontini, G. Tarzia, D. Piomelli, *The 17th European Symposium on Quantitative Structure-Activity Relationships & Omics Technlogies and Systems Biology* (EuroQSAR-08) **2008**, Universitetstryckeriet, Uppsala (Sweden); b) F. Vacondio, C. Silva, A. Lodola, A. Fioni, S. Rivara, A. Duranti, A. Tontini, S. Sanchini, J. Clapper, D. Piomelli, M. Mor, G. Tarzia, *ChemMedChem* **2009**, *4*, 1495 – 1504.
[64] K. Fukui, *Theory of Orientation and Stereoselection*, Springer, New York, **1975**, pp. 34 – 39.
[65] P. Geerlings, F. De Proft, W. Langenaeker, *Chem. Rev.* **2003**, *103*, 1793 – 1873.
[66] A. Golbraikh, A. Tropsha, *J. Comput. Aided Mol. Des.* **2002**, *16*, 357 – 369.
[67] J. T. Leonard, K. Roy, *QSAR Comb. Sci.* **2006**, *25*, 235 – 251.
[68] M. K. McKinney, B. F. Cravatt, *J. Biol. Chem.* **2003**, *278*, 37393 – 37399.
[69] A. Lodola, M. Mor, J. Sirirak, A. J. Mulholland, *Biochem. Soc. Trans.* **2009**, *37*, 363 – 367.
[70] A. N. Jain, *J. Comput. Aided Mol. Des.* **2007**, *21*, 281 – 306.
[71] D. Horvath, F. Bonachera, V. Solov'ev, C. Gaudin, A. Varnek, *J. Chem. Inf. Model.* **2007**, *47*, 927 – 939.
[72] B. L. Bush, R. B. Nachbar, *J. Comput. Aided Mol. Des.* **1993**, *7*, 587 – 619.
[73] A. Golbraikh, A. Tropsha, *J. Mol. Graph. Model.* **2002**, *20*, 269 – 276.
[74] D. M. Hawkins, S. C. Basak, D. Mills, *J. Chem. Inf. Comput. Sci.* **2003**, *43*, 579 – 586.
[75] R. R. Mittal, L. Harris, R. A. McKinnon, M. J. Sorich, *J. Chem. Inf. Model.* **2009**, *49*, 704 – 709.
[76] V. N. Viswanadhan, Y. Sun, M. H. Norman, *J. Med. Chem.* **2007**, *50*, 5608 – 5619.
[77] C. I. Bayly, P. Cieplak, W. Cornell, P. A. Kollman, *J. Phys. Chem.* **1993**, *97*, 10269 – 10280.
[78] F. Lindgren, P. Geladi, S. Rannar, S. Wold, *J. Chemom.* **1994**, *8*, 349 – 363.
[79] R. D. Clark, P. C. Fox, *J. Comput. Aided Mol. Des.* **2004**, *18*, 563 – 576.
[80] A. Tropsha, P. Gramatica, V. K. Gombar, *QSAR. Combinatorial. Science.* **2003**, *22*, 69 – 77.
[81] D. M. Hawkins, *J. Chem. Inf. Comput. Sci.* **2004**, *44*, 1 – 12.
[82] a) W. L. Jorgensen, *Sci. J. Chem. Inf. Model.* **2006**, *46*, 937; b) A. Tropsha, A. Golbraikh, *Curr. Pharm. Des.* **2007**, *13*, 3494 – 3504; c) Organization for Economic Co-operation and Development. Guidance document on the validation of (quantitative)structure-activity relationship ((Q)SAR) models. OECD Series on Testing and Assessment 69. OECD Document ENV/JM/MONO, **2007**, pp. 55–65.
[83] V. N. Viswanadhan, A. K. Ghose, G. R. Revankar, R. K. Robins, *J. Chem. Inf. Comput. Sci.* **1989**, *29*, 163 – 172.
[84] P. J. Goodford, *J. Med. Chem.* **1985**, *28*, 849 – 857.
[85] M. Baroni, G. Costantino, G. Cruciani, D. Riganelli, R. Valigi, S. Clementi, *Quantitative. Structure-Activity. Relationships.* **1993**, *12*, 9 – 20.
[86] J. R. Clapper, F. Vacondio, A. R. King, A. Duranti, A. Tontini, C. Silva, S. Sanchini, G. Tarzia, M. Mor, D. Piomelli, *ChemMedChem* **2009**, *4*, 1505 – 1513.
[87] M. Myllymäki, J. Castillo-Melendez, A. Koskinen, A. Minkkilä, S. Saario, T. Nevalainen, T. Järvinen, A. Poso, O. Salo-Ahen, **2008**, WO2008129129; CAN149:493395.
[88] H. Jones, T.-Y. Shen, *Ger. Offen.* **1971**, DE2130709; CAN76:113209.
[89] R. D. Miller, V. Y. Lee, C. R. Moylan, *Chem. Mater.* **1994**, *6*, 1023 – 1032.
[90] K. Oscarsson, S. Oscarson, L. Vrang, E. Hamelink, A Hallberg, B. Samuelsson, *Bioorg. Med. Chem.* **2003**, *11*, 1235 – 1246.
[91] A. H. Golden, M. Jones, *J. Org. Chem.* **1996**, *61*, 4460 – 4461.
[92] A. McKillop, D. Kemp, *Tetrahedron* **1989**, *45*, 3299 – 3306.
[93] Z. Jayyosi, G. M. McGeehan, M. F. Kelley, R. F. Labaudiniere, L. Zhang, T. J. Caulfield, A. Minnich, M. Bobko, R. Morris, R. D. Groneberg, D. G. Mcgarry, **2000**, WO2000064876; CAN133:335164.
[94] D. Asai, Y. Tahara, M. Nakai, Y. Yakabe, M. Takatsuki, T. Nose, T. Shinmyozu, Y. Shimohigashi, *Toxicol. Lett.* **2000**, *118*, 1 – 2.
[95] M. M. Bradford, *Anal. Biochem.* **1976**, *72*, 248 – 254.
[96] a) A. Lorenzen, M. Fuss, H. Vogt, U. Schwabe, *Mol. Pharmacol.* **1993**, *44*, 115 – 123; b) K. M. Kurkinen, J. Koistinaho, J. T. Laitinen, *Brain Res.* **1997**, *769*, 21 – 28; c) J. R. Savinainen, T. Jarvinen, K. Laine, J. T. Laitinen, *Br. J. Pharmacol.* **2001**, *134*, 664 – 672.
[97] SYBYL v. 8.0, Tripos Associates, Inc., St. Louis, MO (USA).
[98] T. A. Halgren, *J. Comput. Chem.* **1999**, *20*, 720 – 729.
[99] S. C. Lovell, J. M. Word, J. S. Richardson, D. C. Richardson, *Proteins Struct. Funct. Bioinf. Proteins. Zeitschrift wurde erst 2004 gerändet!* **2000**, *40*, 389 – 408.
[100] J. M. Wang, P. Cieplak, P. A. Kollman, *J. Comput. Chem.* **2000**, *21*, 1049 – 1074.
[101] W. Humphrey, A. Dalke, K. Schulten, *J. Mol. Graph.* **1996**, *14*, 33 – 8, 27 – 28.
[102] S. L. Mayo, B. D. Olafson, W. A. Goddard III, *J. Phys. Chem.* **1990**, *94*, 8897 – 8909.
[103] U. C. Singh, P. A. Kollman, *J. Comput. Chem.* **1984**, *5*, 129 – 145.
[104] Gaussian 03, Revision B.04, M. J. Frisch, G. W. Trucks, H. B. Schlegel, G. E. Scuseria, M. A. Robb, J. R. Cheeseman, J. Montgomery, J. A., T. Vreven, K. N. Kudin, J. C. Burant, J. M. Millam, S. S. Iyengar, J. Tomasi, V. Barone, B. Mennucci, M. Cossi, G. Scalmani, N. Rega, G. A. Petersson, H. Nakatsuji, M. Hada, M. Ehara, K. Toyota, R. Fukuda, J. Hasegawa, M. Ishida, T. Nakajima, Y. Honda, O. Kitao, H. Nakai, M. Klene, X. Li, J. E. Knox, H. P. Hratchian, J. B. Cross, V. Bakken, C. Adamo, J. Jaramillo, R. Gomperts, R. E. Stratmann, O. Yazyev, A. J. Austin, R. Cammi, C. Pomelli, J. W. Ochterski, P. Y. Ayala, K. Morokuma, G. A. Voth, P. Salvador, J. J. Dannenberg, V. G. Zakrzewski, S. Dapprich, A. D. Daniels, M. C. Strain, O. Farkas, D. K. Malick, A. D. Rabuck, K. Raghavachari, J. B. Foresman, J. V. Ortiz, Q. Cui, A. G. Baboul, S. Clifford, J. Cioslowski, B. B. Stefanov, G. Liu, A. Liashenko, P. Piskorz, I. Komaromi, R. L. Martin, D. J. Fox, T. Keith, M. A. Al-Laham, C. Y. Peng, A. Nanayakkara, M. Challacombe,

P. M. W. Gill, B. Johnson, W. Chen, M. W. Wong, C. Gonzalez, J. A. Pople, Gaussian, Inc., Wallingford, CT (USA), **2004**.
[105] MOPAC v. 6.0 (QCPE No. 455) interface in SYBYL 8.1.
[106] R. G. Pearson, *J. Am. Chem. Soc.* **1963**, *85*, 3533 – 3539.
[107] R. G. Parr, R. G. Pearson, *J. Am. Chem. Soc.* **1983**, *105*, 7512 – 7516.
[108] T. Koopmans, *Physica* **1934**, *1*, 104 – 113.
[109] R. D. Clark, *J. Chem. Inf. Comput. Sci.* **1997**, *37*, 1181 – 1188.
[110] R. D. Clark, *J. Comput. Aided Mol. Des.* **2003**, *17*, 265 – 275.
[111] Molecular Operating Environment (MOE) 2008.10, Chemical Computing Group, Inc., Montreal (Canada).
[112] G. Klebe, U. Abraham, *J. Comput. Aided Mol. Des.* **1999**, *13*, 1 – 10.
[113] M. Böhm, J. Stürzebecher, G. Klebe, *J. Med. Chem.* **1999**, *42*, 458 – 477.
[114] GRID v 22a, Molecular Discovery, Ltd., Pinner, Middlesex (UK).

Received: September 17, 2009
Revised: November 17, 2009
Published online on December 18, 2009

